



**UNIVERSITY OF NAIROBI**

College of Architecture and Engineering

Institute of Nuclear Science and Technology

**Modeling Trajectories of Electrohydrodynamic Atomization Droplets in Simple-Jet  
Mode: Investigating impact of additional forces**

by:

Ondimu Obed Marube

S56/71535/2014

BSc. Electrical and Electronic Engineering

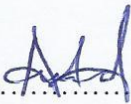
A Thesis submitted in partial fulfillment of the degree of Master of Science in Nuclear Science at the Institute of Nuclear Science and Technology in the University of Nairobi.

© 2018

## Declaration

### Declaration

This thesis is my original work and has not been presented for a degree award any other university.

Sign  ..... Date: 13/02/2018 .....


Ondimu Marube Obed

S56/71535/2014

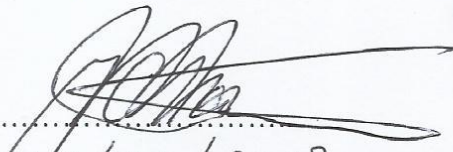
### Supervisors

This thesis has been submitted to the Institute of Nuclear Science and Technology, The University of Nairobi with our approval as supervisors.


Prof. Michael J. Gatari  
Institute of Nuclear Science and Technology  
University of Nairobi, Kenya

Sign  .....  
Date: 14/2/18 .....

Prof. Jan C. M. Marijnssen  
University of Florida, USA and  
Nairobi, Kenya

Sign  .....  
Date: 13/02/2018 .....

Dr. Luewton Lemos Agostinho  
NHL, University of Applied Sciences  
Leeuwarden, Netherlands

Sign  .....  
Date: 13/02/2018 .....

## **Dedication**

To my parents.

## **Acknowledgement**

I take this opportunity to express my profound sense of gratitude and indebtedness to my project supervisors; **Prof. M. J. Gatari**, Professor, University of Nairobi, **Prof. J. C. M. Marijnissen**, Professor, University of Florida, USA and Nairobi, Kenya and **Dr. L. L. F. Agostinho**, Assistant Professor, NHL University of Applied Sciences, and Centre of Expertise Water Technology (CEW), for their invaluable and esteemed guidance, kind cooperation and constructive criticism, constant encouragement and motivation with insightful comments and inspiration during the thesis project work. Without their indomitable scientific temperament and excellent understanding of Electrohydrodynamic Atomization, this work could not have been a success.

Besides my supervisors, I also extend my sincere thanks to **Ir. V. G. Aiyar**, Project Engineer, NHL University of Applied Sciences, for his kind cooperation and guidance in the High Voltage laboratory. I thank **P. Citroen** and **A. Rai**, for their invaluable support and help in the laboratory to carry out experiments.

Special thanks to the Managing Director, **Ir. Q. G. Adema**, and the Office Manager, **Yvette de Vlieg**, Centre of Expertise Water technology (CEW), for giving me the golden opportunity of joining their student-internship program. I am so grateful for their kind support and immense help with the logistics. Sincerely, I thank the International Science Program (ISP), for their fund contribution into this project through their Physics program with the University of Nairobi in the Institute of Nuclear Science and Technology (INST). I thank the Kenya Nuclear Electricity Board (KNEB) for sponsoring my master's degree program.

Last but not least, I wish to express my sincere gratitude to my wife, for her constant motivation and encouragement. Special thanks to my parents as well as brothers and sister, for their precious moral support and encouragement.

# 1 Table of Contents:

Declaration.....	i
Dedication .....	ii
Acknowledgement .....	iii
List of Figures.....	vii
List of Tables .....	x
List of Abbreviations and Acronyms .....	xi
Abstract.....	xii
<b>1 Introduction .....</b>	<b>1</b>
<b>1.1 Background.....</b>	<b>1</b>
<b>1.2 Problem Statement.....</b>	<b>3</b>
<b>1.3 Justification and Significance .....</b>	<b>3</b>
<b>1.4 Scope.....</b>	<b>4</b>
<b>1.5 Objectives.....</b>	<b>4</b>
<b>2 Literature Review.....</b>	<b>5</b>
<b>2.1 Liquid Atomization .....</b>	<b>5</b>
<b>2.2 Electrohydrodynamic Atomization (EHDA) .....</b>	<b>7</b>
<b>2.3 Brief history of Electrohydrodynamic atomization .....</b>	<b>7</b>
<b>2.4 Electro-Spraying Modes .....</b>	<b>8</b>
<b>2.5 Simple-Jet Mode.....</b>	<b>9</b>
<b>2.6 Rayleigh Limit .....</b>	<b>11</b>
<b>2.7 Configurations of Electrospraying .....</b>	<b>11</b>
<b>2.8 Electrospray models in the Cone-jet mode .....</b>	<b>12</b>

2.9	Initial radial displacement of the droplets .....	13
2.10	Gauss law .....	13
2.11	Particle packing factor.....	15
3	Research Methods and Materials .....	16
3.1	Introduction.....	16
3.2	Calculation of the background electric field.....	17
3.3	Experimental Method .....	18
3.4	Image droplet isolation for experimental trajectories .....	19
3.5	Calculation of Droplets' Trajectories.....	20
3.6	Solving the Force Balance Equation.....	22
3.7	Droplet Charge.....	24
3.8	Droplet Deformation.....	24
3.9	Validation.....	25
3.10	Analyzing the force components.....	25
3.11	Analysis of the spray packing factor .....	25
3.12	Investigating the effect of wind on the spray shape .....	27
4	Results and Discussion.....	28
4.1	The Calculated Background Electric Field .....	28
4.2	Experimental results and model input parameters .....	29
4.3	Velocity Profile .....	40
4.4	Force components .....	41
4.5	Representation of forces acting on the droplet.....	43
4.6	Droplets' packing factor .....	45
4.7	The effect of wind on the droplets' trajectories .....	46
5	Conclusion and Recommendations.....	48

<b>5.1</b>	<b>Conclusion.....</b>	<b>48</b>
<b>5.2</b>	<b>Recommendations .....</b>	<b>49</b>
	<b>References .....</b>	<b>50</b>
	<b>Appendix.....</b>	<b>53</b>

## List of Figures

Figure 2-1: Different regimes of droplet formation; (a) Periodic Dripping regime, (b) Dripping Faucet regime, (c) Jetting regime.....	6
Figure 2-2: Schematic diagram of the different Electro spraying modes at different values of the electric potential and liquid flowrate for a given nozzle/counter electrode geometry.....	8
Figure 2-3: Change of mechanism in jet breakup due to increase in applied electric potential. ....	10
Figure 2-4: Different configurations of the nozzle and the counter-electrode in electro spraying; (i) Nozzle/plate, (ii) Nozzle/ringdown, (iii) Nozzle/ringup .....	12
Figure 2-5: Distribution of charge on a prolate shaped sphere. ....	14
Figure 2-6: A sequence of charged spheres: Theory to explain charge distribution on a tear shaped object .....	15
Figure 3-1: A flowchart for the experimental and the modelling steps in this work...	17
Figure 3-2: Defined geometry in COMSOL Multiphysics <sup>®</sup> 4.4 (counter electrode ring (1), nozzle (2), counter electrode support (3) and surrounding environment (4)). .....	18
Figure 3-3: Experimental setup for the visualization of the droplets and the spray. ...	19
Figure 3-4: Algorithm for solving the force balance equation for the droplets .....	21
Figure 3-5: Schematic diagram representing the spray sub-sections where the packing factor was calculated.....	26
Figure 3-6: Experimental setup for analyzing the effect of wind on the spray .....	27
Figure 4-1: A graph showing equipotential lines for the electric field and the surface shows the electric potential .....	28
Figure 4-2: Calculated background electric field for (a) Y-component and (b) X-component respectively .....	29
Figure 4-3: Experimental results for different values of liquid flowrate and applied electric potential; (a) the droplets' average Feret diameter, (b) the droplets' initial velocity, and (c) the jet breakup length. In all cases, the error bars represent the standard deviation, in Figure 14a and Figure 14b, and in Figure 14c it is the percentage error of 10% for each measurement. ....	30



<b>Figure 4-4: Droplets' size distribution for potentials ranging between -5 kV and -9 kV at the flow rates of (a) 285 mL h<sup>-1</sup> (b) 360 mL h<sup>-1</sup>, (c) 440 mL h<sup>-1</sup> for experimental data and (d) for simulated size distribution .....</b>	<b>31</b>
<b>Figure 4-5: A demonstration of charge displacement by images taken by a high-speed camera at a speed rate of 12500 f<sub>ps</sub>; (a) A Section of an intact length, with droplets undergoing deformation after they breakup from the jet, (b) evolution of three droplets in four steps after they breakup from the jet, and (c) displacement of the center of charge (c.o.c) from the center of mass (c.o.m).....</b>	<b>32</b>
<b>Figure 4-6: Displacement of the center of charge in the X and Y directions due to droplet's deformation .....</b>	<b>34</b>
<b>Figure 4-7: Isolation of individual droplets from the images to obtain the experimental droplets' trajectories: (a) a single image of the spray; (b) Experimental droplets' trajectories.....</b>	<b>35</b>
<b>Figure 4-8: General spray shape for the calculated droplets' trajectories at different values of applied electric potential at liquid flowrates .....</b>	<b>36</b>
<b>Figure 4-9: Experimental and theoretical droplets' trajectories for some values of the applied electric potential and liquid flowrate.....</b>	<b>37</b>
<b>Figure 4-10: The spray shapes for (a) the experimental droplet's trajectories, and (b) the calculated droplet's trajectories, the dots indicate the approximated triangular area .....</b>	<b>38</b>
<b>Figure 4-11: Y- cross-sectional area of the electrospray, between the breakup point and a distance of 18 mm from the breakup point for electric potential ranging between -5 kV and -9 kV with the flow rates of 285 mL h<sup>-1</sup>, 360 mL h<sup>-1</sup> and 440 mL h<sup>-1</sup></b>	<b>39</b>
<b>Figure 4-12: Simulated droplet charge as a percentage of its Rayleigh limit.....</b>	<b>39</b>
<b>Figure 4-13: The X-component velocity of droplets at an applied electric potential of -5 kV and liquid flowrate of 285 mL h<sup>-1</sup>; (a) experimental and (b) theoretical. ....</b>	<b>40</b>
<b>Figure 4-14: The Y-component velocity of droplets at an applied electric potential of -5 kV and liquid flowrate of 285 mL h<sup>-1</sup>; (a) experimental and (b) theoretical. ....</b>	<b>41</b>
<b>Figure 4-15: The calculated background electric field force acting on the droplets as they break up from the jet; (a) the X-component and (b) the Y-component .....</b>	<b>41</b>

**Figure 4-16: The calculated inter-droplet coulombic force acting on charged droplets as they move away from the breakup point; (a) the Y-component and (b) the X-component.....42**

**Figure 4-17: The calculated drag force of interaction acting on individual droplets as they move away from the breakup point; (a) the Y-component and (b) the X-component.....43**

**Figure 4-18: A representation of all force components acting on a single droplet within a duration of 20 ms after its generation. ....43**

**Figure 4-19: A representation of the average magnitude of various force components acting on all the individual droplets within a duration of 20 ms after their generation; (a) Y- component, (b) X- component. The error bars represent the standard deviation44**

**Figure 4-20: Graphs showing the variation of the droplets packing factor with distance from the breakup point at an applied electric potential of -6 kV and for different liquid flowrates; (a)  $Q= 285 \text{ mL h}^{-1}$ , (b)  $Q= 360 \text{ mL h}^{-1}$ , (c)  $Q= 440 \text{ mL h}^{-1}$ ..45**

**Figure 4-21: Droplets' trajectories for the flowrate of  $285 \text{ mL h}^{-1}$  and an applied electric potential of -6 kV with an introduced wind; (a) Experimental results and (b) theoretical results, for different values of velocity; (1)  $2 \text{ m s}^{-1}$ , (2)  $4 \text{ m s}^{-1}$ , and (3)  $6 \text{ m s}^{-1}$ 46**

## **List of Tables**

<b>Table 3.1: Properties of the liquid (tap water) used in all the experiments. ....</b>	<b>18</b>
--	-----------

## List of Abbreviations and Acronyms

B	Bond number
$C_D$	Drag coefficient
c.o.c	Center of charge
c.o.m	Center of mass
EHDA	Electrohydrodynamic Atomization
$\epsilon_0$	Electric permittivity of free space
$f_{ps}$	Frames per second
HS	High Speed
HV	High Voltage
J	Jetting regime
K	Liquid electric conductivity
$\eta$	Coefficient of dynamic viscosity
PD	Periodic Dripping
$\rho_{air}$	Air density
$\rho_l$	Liquid density
Q	Liquid flowrate
q	Droplet charge
$\phi$	Electric potential
$r_d$	Droplet radius
Re	Reynolds number
$r_j$	Jet radius
$\gamma$	Liquid surface tension
$\mu$	Dynamic viscosity of air
$v_j$	Jet velocity
$W_e$	Weber number

## **Abstract**

Electrohydrodynamic atomization, or Electro spraying, is a process of implementing electric stresses into a liquid breakup process by the application of a strong electric field ( $\text{kV cm}^{-1}$ ). For a certain spray geometric configuration and a specified liquid, there are different modes of electro spraying depending on the electric field strength and/or liquid flowrate. The cone-jet mode is the most explored one due to its capability of producing highly charged monodisperse droplets in the nano-micrometer size range. This mode is, however, not recommended for systems that depend on electro spray at high throughput. Instead, the simple-jet mode, which operates at much higher flowrates than the cone-jet mode, is recommended for such applications. This mode can also produce monodispersed droplets, but larger than in the former mode for the same liquid properties. This mode is not as much explored as the cone-jet mode. This work was carried out in order to understand the simple-jet mode of electro spray further, so as to design appropriate systems that depend on this mode.

In this work, a physical model for determining the droplet trajectories in the simple-jet mode was designed and implemented. The model was designed to solve the force balance equation, in two dimension (to ensure minimum computational time as opposed to a 3D environment) for each droplet breaking up from the jet. Deformation of the droplets was disclosed to be the major cause of the droplets' initial displacement from the Y- axis. However, a model in a 3D environment is recommended to confirm the findings in this model.

After validating the model, by comparing the theoretical and experimental droplets' trajectories, qualitatively and quantitatively, different components of force acting on the droplets were analyzed. Out of this analysis, an air flow was recommended and investigated to manipulate the droplets' trajectories.

In order to investigate the effect of wind on the droplets' trajectories in the model, the packing factor for the droplets was analyzed. An air flow was then introduced to the spray at a certain point below the breakup point where the packing factor was low. Similar spray deflection was observed in the model and in the experiment. This was after making an assumption of a uniform velocity field for wind in the model.

This model can be used to provide design pre-parameters for those systems that depend on atomization methods at high throughput. It also introduces the possibility of calculating the droplets trajectories with the introduction of extra forces.

# Chapter 1

## Introduction

### 1.1 Background

Electrohydrodynamic Atomization (EHDA), or simply electrospraying, is the process of influencing liquid breakup into droplets, by using a strong electric field ( $\text{kV cm}^{-1}$ ) (Agostinho, 2013). This technology has revolutionized developments in various industrial sectors, such as dry powder production, nano-fiber threads production, non-impact printing, pharmaceuticals delivery in the nano-meter and micro-meter size range, spray painting, applications of pesticides, electroplating, etc. (Geerse, 2003)

In electrospraying, the strong electric field is produced by applying a potential difference between a nozzle and a conductive surface positioned close to it (counter electrode). This is usually performed in three different configurations, i.e. nozzle/ringup, nozzle/ringdown and nozzle/plate (Agostinho, 2013). For each of these configurations, there are different modes of electrospray which can be created depending, basically, on the liquid flow rate, electric field intensity, and liquid properties, such as surface tension, electrical conductivity, electric permittivity, viscosity and density (Hartman, 1998). Cloupeau and Prunet-Foch (1990) were the first authors to classify the different electrospraying modes, relying on the morphology of the meniscus and on the formed jet. Later on, the same authors, as well as Grace and Marijnissen (1994) extended the classification further into dripping, spindle, intermittent cone-jet, cone-jet, and the multiple-jet modes, for low flowrates, and the simple-jet mode, for higher flowrates. Among all these modes, the cone-jet mode is, so far, the most explored. This is due to its capability of producing highly charged monodispersed droplets in the nano-to micro-meter size range. More information about this mode can be found in the literature (Geerse, 2003; Hartman *et al.*, 1999; Yurteri *et al.*, 2010).

Some theoretical investigations have also been conducted to predict some of the electrospray characteristics, such as the droplets' movement, the spray pattern, the liquid breakup process, etc. Most of these investigations, however, are also only done for the cone-jet mode (Agostinho, 2013). Gañán-Calvo *et al.*, (1994) were the first authors to propose an electrospray model using the Lagrangian model of particle motion. The authors

used the momentum equation given by Tchen (1947) and Maxey (1993), taking into account three types of forces, namely; background electric field force, inter-droplet coulombic force between the charged droplets and drag force. Tang and Gomez (1994b) modified this model further by calculating the electric field using the measured droplets' velocities. Grace and Dunn (1996) presented a two-dimensional mathematical model to describe the droplet behavior within an electrodynamic fine spray. Later on, Hartman *et al.*, (1999) modeled the Taylor cone and calculated the spray dispersion. Unlike Gañán-Calvo and Tang, Hartman calculated the background electric field using the Gauss Law and assumed a smaller radial displacement of the droplets at their region of formation. The author also assumed a bimodal droplet size distribution instead of the lognormal droplet size distribution used by Gañán-Calvo. Later on, Geerse (2003) described a three-dimensional model for predicting the droplet dispersion and the deposition region. He calculated the background electric field using FEMLAB<sup>®</sup> software package. Grifoll-Taverna, and Rosell-Llompart (2009), described a numerical model that predicts the spray characteristics in the cone-jet mode, using a nozzle/plate configuration.

The simple-jet mode has not been as highly explored, as the cone-jet mode, both, experimentally and theoretically. However, Agostinho (2013) has recommended this mode for applications that depend on electrospraying at high throughputs, such as spray drying, and desalination systems. He was the first to analyze and characterize this mode. In his work, he defined an operational window in relation to the electric potential and the liquid flow rate for deionized water. He further investigated the effect of liquid electric conductivity on the spray diagram and found out that it only plays a very small role, concerning whipping and dispersion limits. Additionally, he pointed out that the droplet charge can be expressed as a certain percentage of their Rayleigh limit.

In this work a physical model, which can be used to describe the droplet trajectories in the simple-jet mode is presented. The specified input parameters include; initial droplet velocity, average droplet diameter, jet breakup length, liquid flow rate and applied electric potential. In this model, the background electric field is calculated using COMSOL Multiphysics<sup>®</sup> 4.4 software package. The droplets' trajectories are calculated by solving the force balance equation for each droplet, using a MATLAB<sup>®</sup> routine. The input parameters of the model, as well as the real spray pattern used to validate the model, were obtained by



analyzing the images which were taken by a high-speed imaging system.

The model was qualitatively validated by comparing equivalent theoretical and experimental spray shapes, and quantitatively by comparing their X-Y cross-sectional areas respectively. After validating the model, different components of force acting on the droplets were analyzed. The inter-droplet coulombic force was found to be the major component contributing to the droplets' dispersion, while the background electric field force was found to have very little contribution. The model introduces new possibilities of modeling with extra forces.

## **1.2 Problem Statement**

To better understand the properties of the simple-jet mode of electrospray, so as to design appropriate systems, which depend on electrospraying at high throughput, there is an urgent need to come up with a physical model that describes the droplets' trajectories. This model is used to predict the spray dispersion, for a single nozzle system in a nozzle/ringup configuration. This creates new possibilities of designing appropriate systems which depend on electrospray at high throughput, as well as analyzing the effect of additional force components.

## **1.3 Justification and Significance**

Electrospraying has revolutionized developments in various industrial sectors, notwithstanding that it is a relatively new technology in industry. Currently most of its applications are in the cone-jet mode, and as a result more analysis have been carried out on this mode compared to other modes. New applications of Electrospraying, which include desalination and spray drying have been identified, where this mode cannot be relied upon effectively, due to its low throughput. Agostinho (2013) has suggested the simple-jet mode, which has much higher throughput per nozzle as compared with the cone-jet mode, for desalination. As a way of further exploring this mode, to gain more understanding on the relation between spray properties and input parameters, it was necessary to come up with a model which describes the droplets' trajectories in this mode. Appropriate prediction of the spray dispersion, will help in the design of appropriate systems that depend on electrospraying at high throughput.

The presented model introduces design pre-parameters for systems that depend on electrospray at high through put, and verifies the possibility of manipulating the droplet trajectories by extra forces.

## **1.4 Scope**

To carry out laboratory experiments for the simple-jet mode, and model atomized water droplets' trajectories in stagnant air. The contribution of various force components, defining the spray shape, was then investigated. Lastly the effect of wind on the droplets' trajectories was analyzed.

## **1.5 Objectives**

### **1.5.1 Main objectives**

The main objective of this work is to present a physical model capable of predicting the EHDA droplets' trajectories in the simple-jet mode. Electric field characteristics and liquid flow rate are used as the input parameters. This model is for a single nozzle to ring-up configuration. The possibility of manipulating the droplets trajectories was also investigated. This was done by analyzing the contribution of different force components.

### **1.5.2 Specific objectives**

- i. Perform laboratory experiments and obtain images for the spray, used to determine the spray/droplets' properties
- ii. Design a model for calculating the droplets' trajectories in the simple jet mode for stagnant air.
- iii. Model the trajectory of simple jet mode droplets under the influence of an air flow.

## Chapter 2

### Literature Review

#### 2.1. Liquid Atomization

Liquid atomization is the process of dispersing a liquid into small airborne droplets (Ashgriz and Yarin, 2011). The behavior of these particles is often characterized by their sizes. Currently there exist different types of atomizers, the most common types include; pressure, ultrasonic, rotary and electrohydrodynamic atomizers.

Atomization has intrigued scientists since the 15<sup>th</sup> century. Leonardo da Vinci (1490) well noted in his book, ‘the Codex Leicester’ that droplet fall is due to gravitational force overcoming cohesive forces. Later on, Plateau (1873) mentioned that surface perturbations on the cylindrical jet, whose wavelengths are bigger than the jet circumference, make the jet unstable. These perturbations are due to the effects of surface tension forces (Lin, 2003; Hoeve *et al.*, 2010).

Lord Rayleigh (1879) analyzed this phenomenon dynamically and showed that the breakup of an inviscid liquid jet is controlled by the fastest growing wavelength. He also related the liquid jet radius with the droplet radius. He found out that the volume of the pinch-off droplets was approximately  $9\pi r_j^3$ . From where the following relation is derived;

$$r_d = 1.89r_j \dots \dots \dots \text{Equation 2.1}$$

Where;  $r_d$  is the droplet radius and  $r_j$  is the jet radius. This relationship is famously known as the Rayleigh equation. However, this relationship is only applicable in the jetting/Rayleigh breakup regime. This is because the Rayleigh breakup regime has an established jet, unlike the Periodic Dripping (PD) or Dripping Faucet (DF) regime.

Lasheras and Clanet (1999) classified droplet formation mechanisms into three main droplet formation regimes as; Periodic Dripping regime, Dripping Faucet regime and the Jetting (J) regime. These regimes can be determined by the Weber number

$$W_e = \frac{\rho_l v^2 r}{\gamma} \dots \dots \dots \text{Equation 2.2}$$

Where;  $\rho_l$  is the density of the liquid,  $v$  is velocity of the fluid,  $r$  the internal radius of the nozzle and  $\gamma$  is the surface tension of the liquid.

When a liquid is pumped slowly through a nozzle, a pendant droplet with a quasi-static growth is formed. When the gravitational force overcomes the surface tension, the droplet pinches-off from the meniscus. Droplet Formation by this mechanism is referred to as Periodic Dripping regime (Figure 2-1a). By increasing velocity at which the liquid leaves the nozzle, the droplets are slowly turned into a streaming jet. This jet eventually breaks into droplets as it progresses downstream. The continuous length of the jet from the nozzle until the point of droplet formation is referred to as the intact length or breakup length. The schematic diagram in Figure 2-1 shows the different regimes of droplet formation.

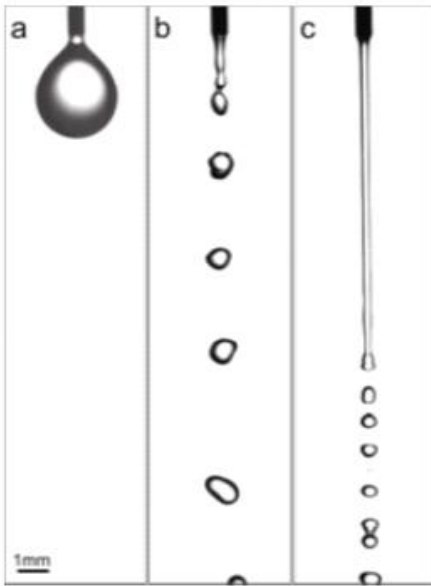


**Figure 2-1: Different regimes of droplet formation; (a) Periodic Dripping regime, (b) Dripping Faucet regime, (c) Jetting regime. (Adopted from Agostinho *et al.*, (2012))**

This intact length increases linearly at first. Droplet formation under this mechanism, when the intact length is growing linearly, is referred to as Dripping Faucet regime (Figure 2-1b). The jet, then increases nonlinearly with increase in liquid velocity. Droplet formation under this mechanism is referred to as jetting regime ( $W_e > 4$ ) (Figure 2-1c).

Further increase in liquid flowrate, beyond what is required for the formation of the jetting regime, results into an increase of aerodynamic effects. This effects accelerate the liquid breakup process. Therefore, droplet formation under this mechanism is referred to as the wind-induced regime (Agostinho, 2013). This regime occurs when the flow rate is increased beyond the jetting regime (Hoeve *et al.*, 2010).

## **2.2. Electrohydrodynamic Atomization (EHDA)**

Electrohydrodynamic atomization, basically, consists of the application of a strong electric field to influence the breakup of a liquid jet from capillaries (Tang and Gomez, 1994c). This technique can generate large amount of charged droplets with relatively narrow size distribution. In this process the droplet size can be varied by changing the electric field strength, the liquid flow rate, and the properties of the liquid (Agostinho 2013, Grace and Marijnissen, 1994).

## **2.3. Brief history of Electrohydrodynamic atomization**

William Gilbert (1600) mentioned the effect of an electric field on a liquid meniscus, back in the sixteenth century. In his work, “*De Magnete*”, Gilbert mentioned that when a piece of amber is brought close to a water droplet standing on a dry surface, the water droplet changes its spherical shape into a conical shape. Later on, Zeleny (1915) investigated the droplet instability and found out that when a liquid meniscus is subjected to a strong enough electric field, it turns into a conical shape and emits some mist. Thereafter, Taylor (1969) developed the first mathematical model which described the conical shape formed by the liquid meniscus on the application of a strong electric field, by balancing the existing forces.

Tang and Gomez (1994c) did an analysis on the electrospray of monodispersed water droplets and found out that; the droplet size can be solely controlled by the flow rate, and that the addition of salt to pure water reduces droplet size at a constant flow rate. Later on, in the same year, Cloupeau and Plunet-Foch (1994) came up with a designation for various modes of drop formation. They designated the modes as follows; cone-jet and its variants, pulsed cone-jet, multijet microdripping, ramified-jet, simple-jet and spindle jet modess. Subsequently, Grace and Marijnissen (1994) further extended this classification of the mode. Hartman *et al.*, (1999) carried out an investigation on the parameters that determine the droplet size in the cone jet mode and identified the following parameters; liquid flow rate, conductivity, surface tension, density, viscosity, ion species in the liquid, electric potential and electrode configuration.

Agostinho (2013) characterized the simple-jet mode for inviscid liquids based on two control parameters; the flow rate and the electric field. They further investigated on vaporization enhancement by the application of the Electro spraying atomization technique in the simple-jet mode.

## 2.4. Electro-Spraying Modes

The most used definition of electro spraying modes was first done by Cloupeau and Prunet-Foch (1994). The authors defined these modes by their multiple characteristics without a well-defined transition between them. Later on, Grace and Marijnissen (1994) extended these classification further. Figure 2-2 shows a schematic diagram of the classification of electro spraying modes as proposed by Agostinho (2013).

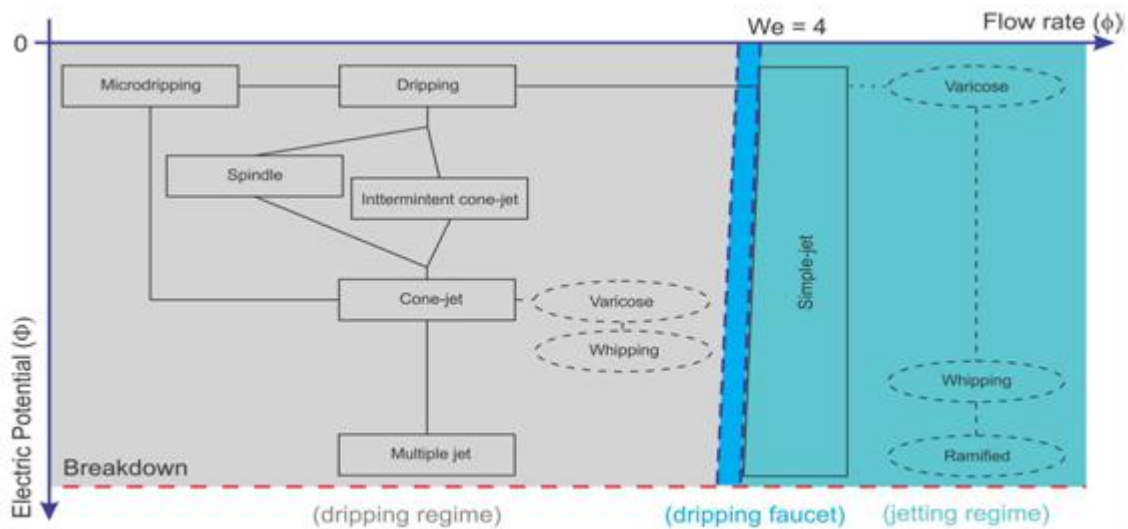


**Figure 2-2: Schematic diagram of the different Electro spraying modes at different values of the electric potential and liquid flowrate for a given nozzle/counter electrode geometry. (Adopted from Agostinho (2013))**

The dripping mode is characterized by the production of droplets with larger diameter than the nozzle inner diameter at low potential and low flowrate ( $We < 2.5$ ). The frequency of droplet formation in this mode increases with increase in an applied electric potential. An increase in electric potential changes the dripping mode into spindle mode or intermittent cone-jet mode. In both of these two modes, large and small droplets are formed alternately. In the spindle mode, small droplets are formed from a jet which appears at the tip of the liquid ligament. The ligament eventually breaks up into (alternate) big and small droplets

(usually referred to as satellite droplets). In the intermittent cone-jet mode, a cone-jet spraying is followed by the ejection of larger droplets.

When the applied electric field is increased in both the spindle mode and the intermittent cone-jet mode, the spray turns into cone-jet mode. This mode is characterized by the formation of very small droplets breaking out from a ligament that originates from the Taylor cone. This ligament breaks up into fine droplets, mainly, due to Plateau-Rayleigh instabilities, i.e. varicose breakup. Further increase in potential, within the same window of the cone-jet mode, causes the breakup to be influenced by kink instabilities, i.e. whipping breakup. Further increase in electric potential, leads to the formation of the multi-jet mode, whereby multiple jets originate from the liquid meniscus. If the flow rate is decreased further from the Dripping mode, the Micro dripping mode, which is associated with the formation of a smaller diameter than the nozzle inner diameter, may occur (Agostinho *et al.*, 2012).

When the flow rate is increased further into the jetting regime, i.e.  $W_e > 4$ , the simple-jet mode is formed (Agostinho *et al.*, 2012). Given its importance in this work, it will be further described in the next section

## **2.5. Simple-Jet Mode**

The Simple-jet mode was first characterized by Agostinho (2013). This mode is characterized with a higher throughput, when compared to the cone-jet mode which is highly explored. The former is therefore, recommended for applications which depend on atomization at high flowrate. In this mode, droplets are formed from the breaking up of a liquid jet, just like in the cone-jet mode. Besides the flowrate, another difference between these two modes is that, in the cone-jet mode the jet originates from the tip of the Taylor cone, while in the simple-jet mode, it originates directly at the nozzle tip (Agostinho, 2013). Figure 2-3 shows the different regimes of droplet formation in the Simple-jet.

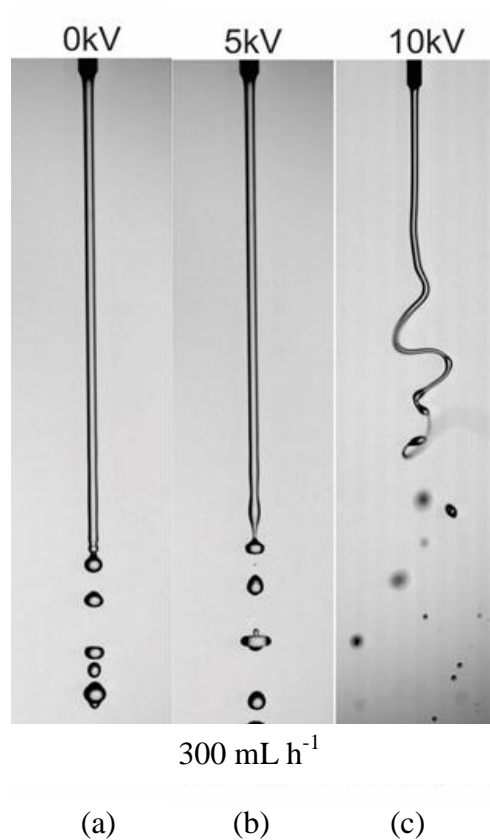


**Figure 2-3: Change of mechanism in jet breakup due to increase in applied electric potential. (Adopted from Agostinho *et al.*, (2012))**

At very low electric potential, the breakup of the simple-jet is not so much different from that of the uncharged jet (Figure 2-3a). This breakup is referred to as varicose breakup. The application of an electric field onto a liquid jet, induces electric surface charge on the jet. Coulombic repulsion between these induced surface charges, leads to an imbalance between pressure, inside the droplet, and surface tension. This imbalance will influence the breakup by increasing its frequency (Figure 2-3b). Further increase in electric potential will lead to off-axis instability, which makes the jet whip and break up into droplets (Figure 2-3c). This breakup of the jet is called whipping breakup.

If the electric potential is increased further, secondary jets issue from the surface of the primary jet. This is called simple-jet mode with ramified breakup (Grace and Marijnissen, 1994). This research will be carried out only for simple-jet with varicose breakup.



## 2.6. Rayleigh Limit

The Rayleigh limit is the maximum amount of charge a droplet can hold without breaking up due to inter-charge repulsion (Tang and Gomez, 1994a). It was named after lord Rayleigh who performed a series of experiments to explain the phenomenon. The limiting charge is given by;

$$Q_R = \pi(8\epsilon_0\gamma D_R^3)^{1/2} \dots\dots\dots\text{Equation 2.3}$$

Where:  $D_R$  is the droplet diameter,  $\gamma$  is the liquid surface tension and  $\epsilon_0$  is permittivity of free space.

When there are surface charges on the droplet, they will be naturally repelling each other. Liquid surface tension will be preventing the droplet from splitting apart. However, if the surface charge is increased beyond the Rayleigh limit, the coulombic force of repulsion will overcome the surface tension and the droplet will eventually disrupt into smaller droplets. Surface charge density decreases with increase in surface area. The effective surface area of the droplet increases when it splits up. With decrease in surface charge density, the liquid surface tension will overcome the coulombic force, and therefore the resulting droplets will be stable. Agostinho *et al.*, (2012) characterized the droplets generated in the Simple-jet mode to have a charge ranging between 5% and 10% of their Rayleigh Limit.

## 2.7. Configurations of Electrospaying

There are three common electrospaying configurations, namely; (i) nozzle/plate, (ii) nozzle/ringdown and (iii) nozzle/ringup (Figure 2-4). The nozzle to plate configuration is the classical one. The nozzle is kept perpendicular to the plane of the plate surface at some distance from the plate, and an electric potential is established between the nozzle tip and this plate. This configuration is not always desirable because droplets accumulate on the counter-electrode (plate) surface and disturb the characteristics of the electric field. Additionally in this configuration, the droplets cannot be available after electrospaying. The nozzle/ringdown can generate the necessary electric field required to cause the droplets dispersion, with a reduced accumulation on the counter electrode as compared to the nozzle/plate configuration. This results into reduced interference on the electric field, and droplets are free, after electrospaying, to disperse over a wider area (Geerse, 2003).

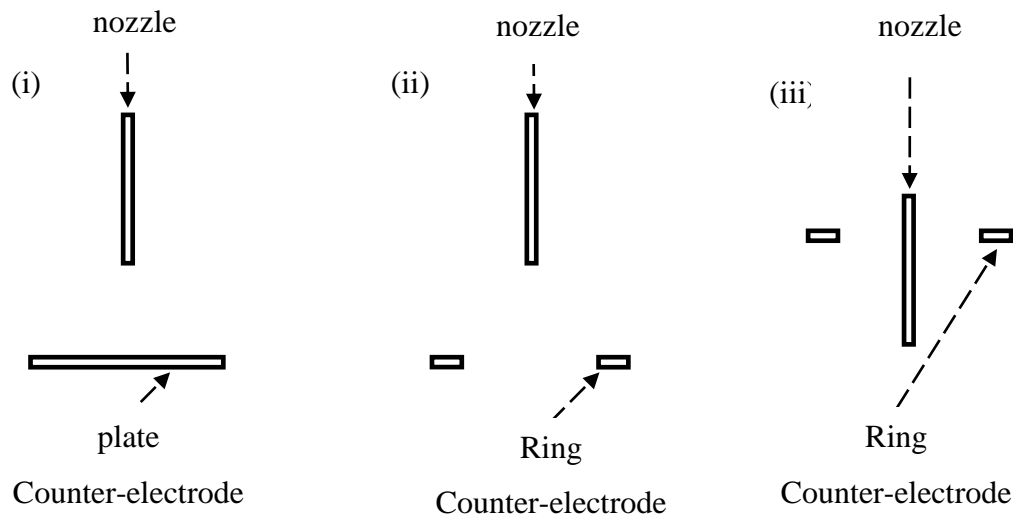


**Figure 2-4: Different configurations of the nozzle and the counter-electrode in electrospaying; (i) Nozzle/plate, (ii) Nozzle/ringdown, (iii) Nozzle/ringup**

The Nozzle/ringup configuration was proposed by Geerse (2003) to further solve the problem of droplet accumulation on the counter electrode surface, and its effect on electric field characteristics. It is also possible to make an insulated device in this configuration. Here the counter electrode ring is kept above the nozzle tip. However, when there are very small droplets, referred to as satellite droplets, because of their small inertia, they can follow the electric field lines and settle on the surface of the counter electrode. In such cases some insulation means has to be provided to avoid short circuit and interference on the electric field characteristics. The electric potential can be applied on the nozzle as well as on the counter-electrode. This also prevents the accumulation of droplets on the counter-electrode. In this work, a single nozzle system in the nozzle/ringup configuration was used

## 2.8. Electrospay models in the Cone-jet mode

The Lagrangian model can be used to describe the dynamics of droplets moving in a fluid, by tracking multiple droplets, solving the momentum equation of each individual particle (Zhang and Chen, 2007). Using this model, Gañán-Calvo (1994) derived a model that describes the motion of highly charged droplets within a strong electric field from the momentum equation given by Tchen (1947) and Maxey (1993), taking into account four types of forces, namely; gravity, electric field, inter-droplet coulombic force between the charged droplets and drag. Tang and Gomez (1994b) modified this model further. They calculated the electric field using the measured droplets' velocities. Grace and Dunn (1996)

presented a two dimensional mathematical model to describe the droplet behavior within an electrodynamic fine spray. Later on, Hartman (1998) modeled the Taylor cone and calculated the spray dispersion. Unlike Gañán-Calvo and Tang, Hartman calculated the background electric field using Gauss Law and assumed a smaller radial droplet displacement at the droplet formation region. The author also assumed a bimodal droplet size distribution instead of the lognormal droplet size distribution used by the former. Later on, Geerse (2003) described a three dimensional model for predicting the droplet dispersion and the deposition region. He calculated the background electric field using FEMLAB<sup>®</sup> software package. Grifoll-Taverna, and Rosell-Llompart (2009) described a numerical model that predicts the spray characteristics in this mode with a nozzle to plate configuration.

## **2.9. Initial radial displacement of the droplets**

The initial displacement of an EHDA droplet from the Y- position is a commonly discussed topic by many authors. Ganan-Calvo (1994), in his model of the cone-jet mode, mentioned about these random perturbations and claimed that the results were not sensitive to the initial position of droplet seeding, provided that the displacements were smaller than the jet radius. Hartman *et al.*, (1998) observed that in the same mode, below a certain flowrate, these displacements are small in comparison with the jet radius for a jet breaking up due to varicose instabilities. However, when the liquid flow rate is increased, kink instabilities become more dominant and hence these random displacements are increased. Therefore, both of them implemented random radial displacement of the droplets in the seeding region to initiate their dispersion. Geerse (2003) attributed the spray formation to changes in the droplets' initial velocity vector as a result of their small displacements. Grifoll-Taverna and Rosell-Llompart (2009) also assumed a random radial displacement of the droplets, in their region of formation, to initiate their dispersion.

## **2.10. Gauss law**

The Gauss law states that if a sphere is assumed to enclose charge, the total electric flux passing through the surface of the sphere is equivalent to the total charge enclosed by the sphere (David *et al.*, 1997). For the case of a uniformly charged sphere, the electric flux passing through the surface of the sphere will be uniformly distributed. To obtain the value of electric field at any point outside the sphere, a spherical surface known as the Gaussian

surface is assumed around the sphere, through the point of interest. The formed Gaussian sphere is centered at an assumed center of charge (center of the Gaussian sphere). Unlike the case of a uniform sphere, where the center of charge coincides with the center of mass, in the case of non-uniform spherical shapes, the center of charge is not located at its center of mass (Bhattacharya, 2010). This is attributed to the non-uniform distribution of charge on such surfaces. Charge density on the surface of a tear shaped body increases with decrease in radius of curvature (Fricker, 1989), as shown in Figure 2-5.

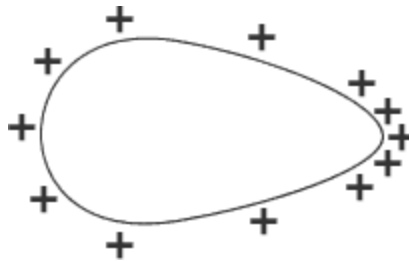


**Figure 2-5: Distribution of charge on a prolate shaped sphere. (Adopted from Splung 2016)**

The droplets undergo shape deformation as they breakup from the jet. This deformation is a well-known subject described by many authors. It can be caused by surface waves due to energy release after break up in the case of uncharged droplets (Klaseboer *et al.*, 2014), also due to charge induction/polarization caused by external electric fields, in the case of charged droplets (Corson *et al.*, 2014, Grimm and Beauchamp 2005). A charged droplet in an electric field, thus, may undergo egg- or tear-shape which would also lead to a non-uniform surface charge distribution as shown in Figure 2-5. Wetzel and Tucker (1999) also presented that the droplets undergo deformation by elongating, tumbling and oscillating between prolate and oblate shape as they move away from the breakup point. This deformation was hypothesized in this work to cause non-uniform distribution of the surface charge. This phenomenon can be explained by the theory of sequence of charged spheres, as shown in Figure 2-6, which states that an electrically conducting tear shape object can be represented by a sequence of touching spheres that are at a common potential ( $V$ ). Since surface charge density ( $\sigma$ ) can be relate to the sphere's radius ( $r$ ) as  $\sigma \propto V \cdot r^{-1}$ , it is evident that surface charge density increases with decrease in radius of the sphere, because all the spheres are at the same potential ( $V$ ) (Fricker, 1989).

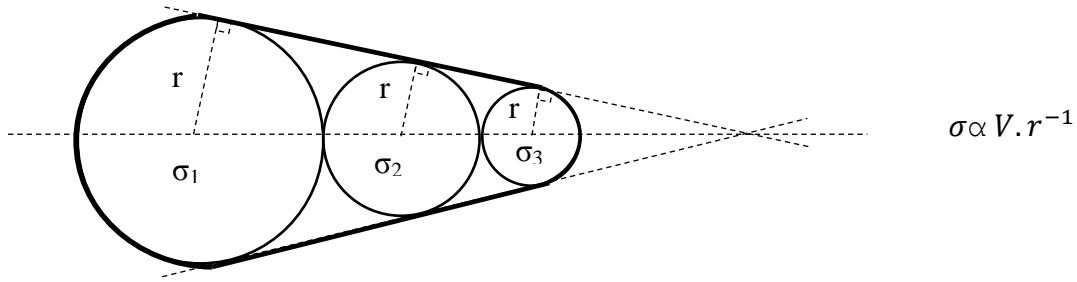


**Figure 2-6: A sequence of charged spheres: Theory to explain charge distribution on a tear shaped object**

This non-uniform distribution of charge on the droplet, causes the center of the Gaussian sphere, where all the droplet charge is assumed to be concentrated, to be displaced from its center of mass (David *et al.*, 1997). The electric forces, acting on the droplet, are concentrated at this point, and as a result the droplet experiences substantial X-component force from the jet as well as the other droplets on the axis. This may cause their initial displacement from the axial position. Once displaced from the axial position, the X-component of force increases gradually.

This droplet deformation was, therefore, presumed in this work as the major cause of the droplet's initial displacement from the axial position. As the droplet's shape changes periodically, the droplet's center will change as well.

### 2.11. Particle packing factor

Packing factor is the fraction of volume occupied by constituent particles to the overall volume of the cloud, whereby a cloud can be considered as the region enclosed by the boundary between where the particles exist and the outer region. If air is blown at the cloud it can either pass inside or outside the cloud depending on the relative resistance between these two paths. This resistance is dependent on the volume fraction/packing factor. When air passes through, all particles experience the same wind velocity, and the overall drag is the sum of all the individual drag experienced by all particles (Hinds, 1999). When air passes around the cloud due to the shadowing effect by some particles on other particles, some extra parameters are used to approximate the drag force (Fuchs, 1964).

## Chapter 3

### Research Methods and Materials

#### 3.1. Introduction

The adopted method for constructing and validating the model can be simplified into the following steps: data acquisition, calculation of the droplets' trajectories, validation of the model, analyzing various force components and investigating the effect of wind on the droplets' trajectories. Data acquisition was done by both calculating the background electric field using COMSOL Multiphysics<sup>®</sup> 4.4. Other input parameters such as the droplets' initial velocity, droplets' average Ferret diameter, droplets' size distribution and the jet breakup length, were obtained through laboratory experiments. Sequentially, these input parameters were used to calculate the droplet trajectories and consequently, the spray patterns using a MATLAB<sup>®</sup> routine. The model was validated by comparing theoretical spray patterns to their equivalent experimental spray patterns. This process was done for different configurations of liquid flowrate and applied electric potential. In the validation phase, whenever a deviation of more than 10% was found, the droplets' charge was adjusted in the model and the trajectories were calculated again. Finally, various force components acting on a single droplet were analyzed and then the effect of air flow investigated. A more illustrative view of the followed steps is as shown by the flowchart in Figure 3-1.

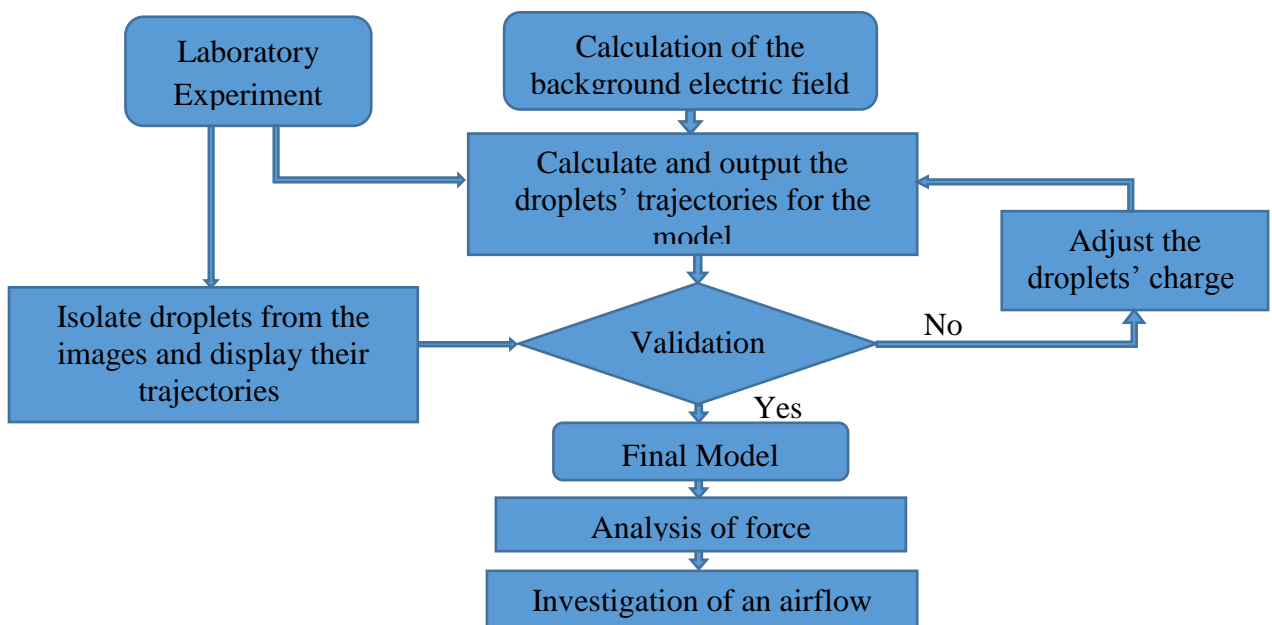


**Figure 3-1: A flowchart for the experimental and the modelling steps in this work.**

### **3.2. Calculation of the background electric field**

Background electric field, which is due to applied electric potential, was calculated as a function of the setup geometry using COMSOL Multiphysics<sup>®</sup> 4.4 software package. The process involved defining the geometry for a single nozzle/ringup configuration (Figure 3-2), similar to the one which was used for all the experiments. Even though it is known that the best environment in this case would be a 2D axisymmetric or a 3D. However, as will be also further commented, to take advantage of the known symmetry of EHDA sprays and make the model simpler, a 2D environment was opted for. Additionally, the validation technique which was to be used to verify the final trajectories of the droplets was also a two dimensional technique. Therefore, this definition of geometry was done using the 2D space dimension package in the electrostatics interface of the AC/DC module, for the scenario of a stationary study. The geometry was defined with a nozzle of outer diameter (OD) of 0.51 mm and an inner diameter (ID) of 0.25 mm. The distance between the nozzle tip and the counter electrode ring was set as 17 mm. Materials were defined using the in-built COMSOL Multiphysics<sup>®</sup> 4.4 Material library in the following way: copper was used for the counter electrode ring, stainless steel 405 annealed for the nozzle, FR4 (circuit board) for the counter electrode support, and finally, air was used for the surrounding environment.

The electrostatics boundary conditions for the geometry were defined as; ground for the nozzle (with zero potential), electric potential for the counter electrode (whose value was varied between -5 kV to -9 kV in steps of -1 kV), dielectric shielding for the circuit board and zero charge for the exterior boundaries.

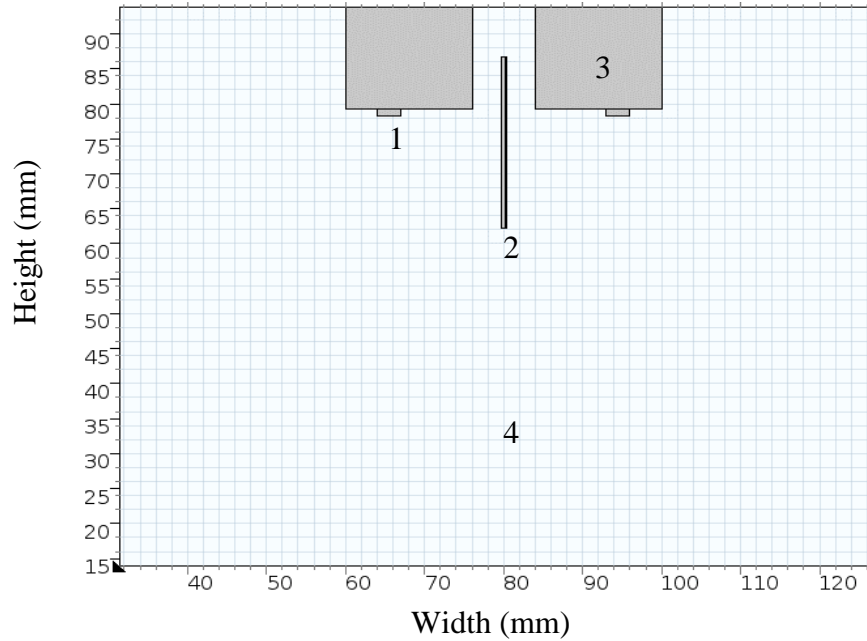


**Figure 3-2: Defined geometry in COMSOL Multiphysics<sup>®</sup> 4.4 (counter electrode ring (1), nozzle (2), counter electrode support (3) and surrounding environment (4)).**

The model in COMSOL Multiphysics<sup>®</sup> 4.4 software package was used to compute the background electric field for different values of applied electric potential, and then the obtained results exported to MATLAB<sup>®</sup>, where a routine was used to extract the background electric field values ( $E(x,y)$ ) at every position inside the geometry as shown in Figure 3-2 above.

### 3.3. Experimental Method

To obtain the input parameters for the model, a single nozzle/ringup setup was built as shown in Figure 3-3 with the same dimensions as highlighted in the previous section. A pump type, MasterFlex<sup>®</sup> Console Drive was used to pump the liquid at a constant flow rate through the nozzle. The liquid used in all experiments was tap water. Its properties are as shown in Table 3.1

**Table 3.1: Properties of the liquid (tap water) used in all the experiments: adopted from Agostinho *et al.*, (2012)**

Liquid property	Viscosity, $\mu$ [Ns m <sup>-2</sup> ]	absolute density, $\rho$ [kg m <sup>-3</sup> ]	surface tension, $\gamma$ [N m <sup>-1</sup> ]	electrical conductivity, K [S m <sup>-1</sup> ]	relative permittivity, $\epsilon$
Value	$1.00 \times 10^{-3}$	$1.00 \times 10^3$	$7.19 \times 10^{-2}$	$5.00 \times 10^{-3}$	$8.01 \times 10^1$



The experiments were performed in three different categories with the flowrates;  $285 \text{ mL h}^{-1}$ ,  $360 \text{ mL h}^{-1}$  and  $440 \text{ mL h}^{-1}$ , i.e. the jetting regime of droplet formation in all experiments. The high voltage was applied to the counter electrode (FUG HCP 14-20000 DC high voltage power supply), while the nozzle was grounded in all the experiments. The values varied between -5 kV and -9 kV in steps of -1 kV for each flowrate.

In order to visualize the droplets and the spray, an imaging system consisting of Photron<sup>®</sup> SA-X2 high-speed camera with a NAVITAR<sup>®</sup> microscopic lens was used with a Dedocool<sup>®</sup> backlight illumination as shown in Figure 3-3.

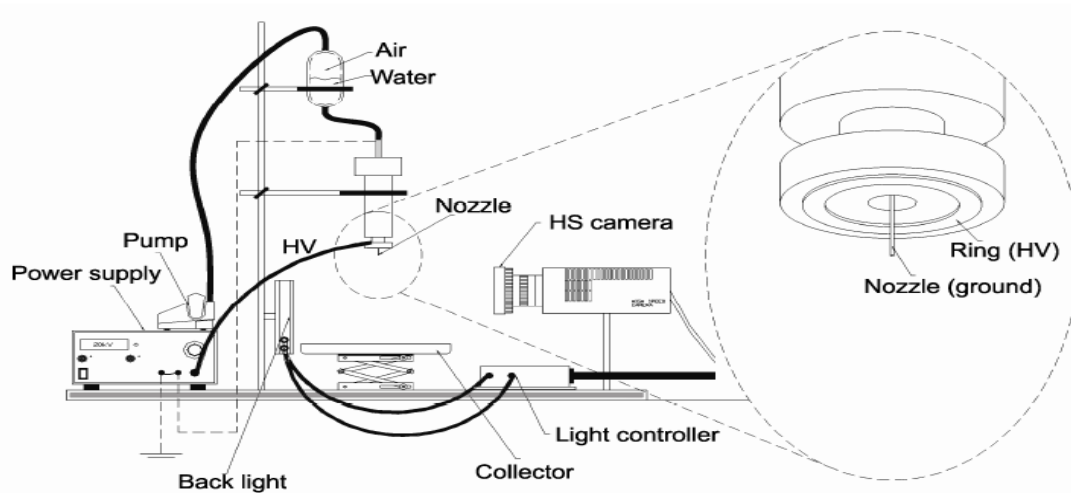


**Figure 3-3: Experimental setup for the visualization of the droplets and the spray.** (Source: Agostinho *et al.*, (2012))

The images were recorded at a constant frame rate ( $12500 \text{ f}_{ps}$ ) and then processed using ImageJ<sup>®</sup> software together with a MATLAB<sup>®</sup> routine. The process comprised of isolating the individual droplets and analyzing some of their properties, such as; initial velocity, deformation and size distribution. This was followed by obtaining their trajectories and finally the spray shape which was used in the validation phase.

### 3.4. Image droplet isolation for experimental trajectories

A MATLAB<sup>®</sup> routine was used to isolate the individual droplets, after performing image analysis. This routine was used to calculate droplets' velocity and display their trajectories. To achieve this, two matrices for X and Y components were defined as follows;

$$\mathbf{X} = \begin{bmatrix} \mathbf{X}_{ij} & \dots & \mathbf{X}_{im} \\ \dots & \dots & \dots \\ \mathbf{X}_{nj} & \dots & \mathbf{X}_{nm} \end{bmatrix} \dots \dots \dots \text{Equation 3.1}$$

And

$$\mathbf{Y} = \begin{bmatrix} \mathbf{Y}_{ij} & \dots & \mathbf{Y}_{im} \\ \dots & \dots & \dots \\ \mathbf{Y}_{nj} & \dots & \mathbf{Y}_{nm} \end{bmatrix} \dots \dots \dots \text{Equation 3.2}$$

*i* Represents the number of time the droplet was appearing in the Field of interest (FOI), up to *n* times, whereas *j* represents the droplet index number up to *m*, the total number of droplets.

The droplet displacement matrix was defined according to;

$$\mathbf{S}_{ij} = \sqrt{(\mathbf{X}_{ij} - \mathbf{X}_{i,j-1})^2 + (\mathbf{Y}_{ij} - \mathbf{Y}_{i,j-1})^2} \dots \dots \dots \text{Equation 3.3}$$

And the matrix of the velocity to be used for validation was obtained by the following equation;

$$\mathbf{V}_{ij} = \mathbf{S}_{ij} \cdot \mathbf{f}_{ps} \dots \dots \dots \text{Equation 3.4}$$

Where;  $f_{ps}$  is the camera frame rate at which the images were taken.

The experimental droplets' trajectories (change of the individual droplets' position) were obtained by plotting the Y-component matrix against the X-component matrix for each droplet. The experimental spray shapes were compared to the modelled one.

### 3.5. Calculation of Droplets' Trajectories

After the background electric field and initial conditions were determined for the droplets, a MATLAB<sup>®</sup> routine was used to solve the force balance equation and output the droplets' trajectories. The routine was according to the flow chart presented in Figure 3-4.

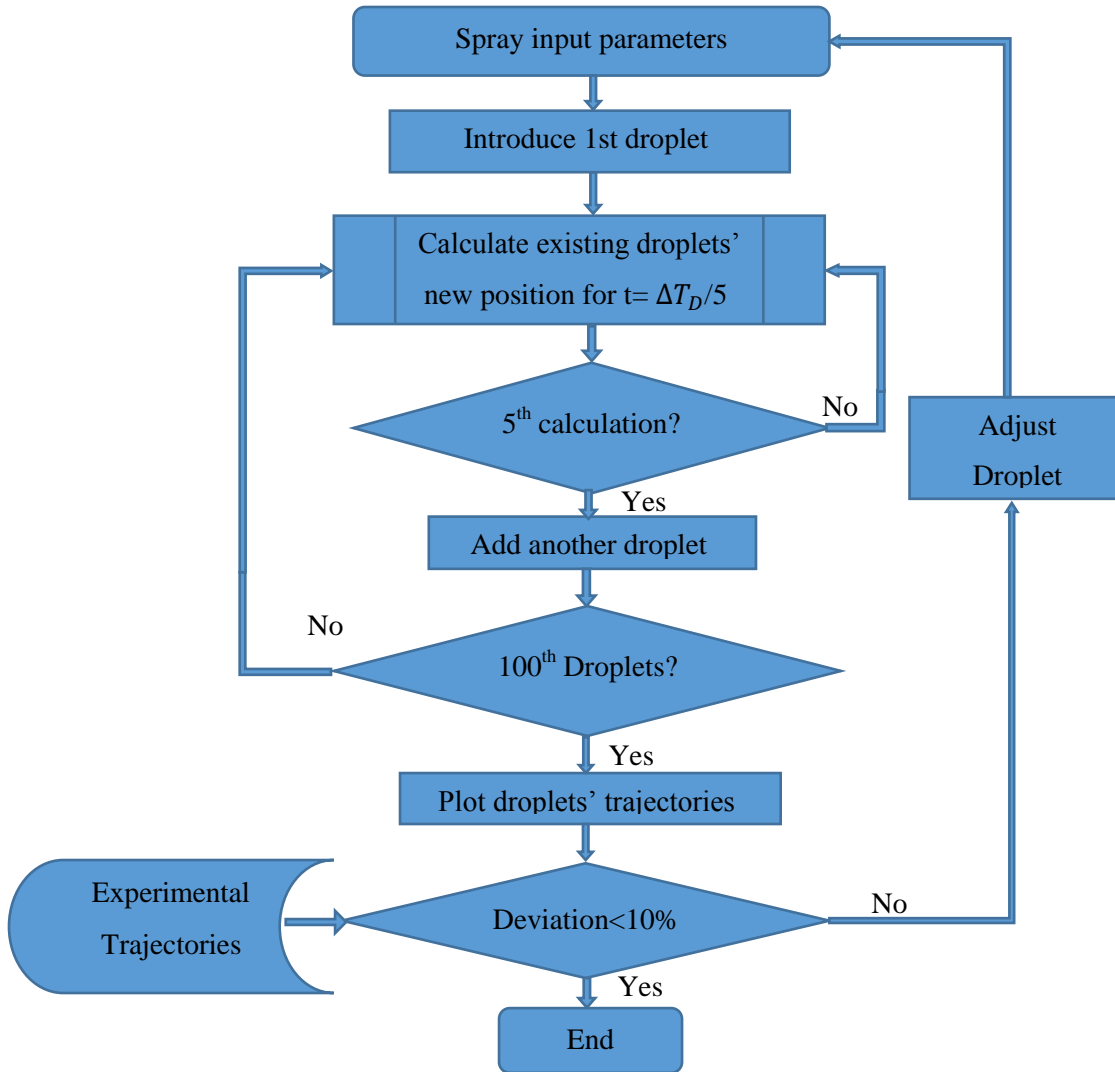


**Figure 3-4: Algorithm for solving the force balance equation for the droplets**

The force balance was performed by starting with an initial droplet at a pre-defined position. For accuracy, the droplet was then moved five steps before the next droplet was introduced. This was done by taking a constant time step, whose value was one-fifth of the time interval between the formation of two droplets (the time interval varied with the liquid flowrate). The process was repeated until the desired number of droplets was reached. In order to calculate the background electric field force and define the inter-droplet coulombic force, the droplet's position was considered. The droplet's deformation and reorientation was simulated by implementing a random displacement on the droplet's center of charge, whose maximum value was obtained through fitting.

The droplets' charge was approximated by using the percentage of the Rayleigh limit, which was presented by Agostinho *et al.*, (2012) to range between 5 and 10%. The entire process was repeated until the right dispersion for the model droplets' trajectories could be obtained. A more detailed explanation about solving the force balance equation is presented in the next section.

### 3.6. Solving the Force Balance Equation

The calculation of the electrosprayed droplets' trajectories, and hence the spray shape for the model, involved solving the force balance equation (in a xy geometry) for each droplet breaking up from the jet. This equation takes into consideration the gravitational force ( $\vec{F}_g$ ), the inter-droplet coulombic force ( $\vec{F}_C$ ), the background electric field force ( $\vec{F}_E$ ) and the drag force ( $\vec{F}_D$ ). They are defined as follows;

**(i) Gravitational force**

Gravitational force is the product between the mass of the droplet and the gravitational acceleration. It is defined by equation 3.5.

$$\vec{F}_i^G = \frac{\pi \cdot \rho_i \cdot d_i^3}{6} \cdot \vec{g} \dots \dots \dots \text{Equation 3.5}$$

Where;  $\rho_i$  is the droplet density and  $d_i$  is the droplet diameter.

**(ii) Inter-droplet coulombic force**

In electrospray, each droplet experiences repulsion from the other droplets due to the presence of surface charge. The resultant repulsive force on each droplet is obtained by taking the vectorial sum of all the inter-droplet coulombic forces acting on that droplet, from the other droplets in the x-y plane. It is defined as:

$$\vec{F}_{i(x,y)}^C = q_i \cdot \sum_{\substack{j=1 \\ j \neq i}}^N \frac{q_j \cdot \vec{r}_{ij}}{4\pi\epsilon_0 \cdot r_{ij}^3} \dots \dots \dots \text{Equation 3.6}$$

Where  $i$  and  $j$  denote the droplet number,  $q$  the droplet charge,  $r_{ij}$  the distance between the two droplets,  $i$  and  $j$ .  $\epsilon_0$  is the absolute permittivity of free space.

**(iii) Background Electric field force**

Background electric force due to the interaction of background electric field and the droplet charge is defined by:

$$\vec{F}_{i(x,y)}^E = q_i \cdot \vec{E} \dots \dots \dots \text{Equation 3.7}$$

(iv) **Drag force**

This is the resistance between the droplet and the surrounding air. Most of the droplets were moving in the Newtonian regime. The drag force, in this regime, is defined by:

$$\vec{F}_{i(x,y)}^D = C_D \cdot \frac{\pi}{8} \cdot \rho_{air} \cdot d_i^2 \cdot (\vec{v}_{air} - \vec{v}_i) \cdot |\vec{v}_{air} - \vec{v}_i| \dots \dots \dots \text{Equation 3.8}$$

Where;  $v_i$  is the velocity of the particle in air,  $v_{air}$  is air velocity,  $d_i$  the particle diameter,  $\rho_{air}$  is air density and  $C_D$  is the drag coefficient.  $C_D$  is determined by the regime in which the droplet is moving. The regime in which the droplet is moving is defined by its Reynolds number, which is calculated as:

$$Re = \frac{\rho_{air} |\vec{v}_{air} - \vec{v}_i| d_i}{\eta_{air}} \dots \dots \dots \text{Equation 3.9}$$

If  $Re \leq 1$  (Stokes regime) the drag coefficient is calculated as:

$$C_D = \frac{24}{Re} \dots \dots \dots \text{Equation 3.10}$$

For  $1 > Re \leq 1000$  (Newtonian regime) the drag coefficient is given by:

$$C_D = \frac{24}{Re} (1 + 0.15Re^{0.687}) \dots \dots \dots \text{Equation 3.11}$$

Most of the presented droplets existed in the Newtonian regime (Hinds, 1999).

The resulting force was calculated for the theoretical droplets and their movement investigated in both (x and y) directions using Newton's law of motion.

$$\begin{aligned} \vec{F}_{Ri(x,y)} = & \mathbf{q}_i \cdot \vec{E} + \mathbf{q}_i \cdot \sum_{j=1}^N \frac{q_j \cdot \vec{r}_{ij}}{4\pi\epsilon_0 \cdot r_{ij}^3} + C_D \cdot \frac{\pi}{8} \cdot \rho_{air} \cdot d_i^2 \cdot (\vec{v}_{air} - \vec{v}_i) \cdot |\vec{v}_{air} - \vec{v}_i| + \\ & \frac{\pi \cdot \rho_i \cdot d_i^3}{6} \cdot \vec{g} \dots \dots \dots \text{Equation 3.12} \end{aligned}$$

Furthermore, the following assumptions were taken on the droplets;

- They were moving in stagnant air.
- They were not evaporating/ coagulating, and thus the droplets' mass remained constant over time
- They had a constant charge

A specific droplet population was defined with a size distribution similar to the experimental droplet population. This definition was done by systematically sampling the experimental population into six groups with an interval of 100  $\mu\text{m}$ . The droplets were then

generated randomly within a given interval with a similar percentage as for the experimental droplet population. A total population of 100 droplets were used in the model. The next step was defining the necessary time interval between which two droplets form. This time interval was experimentally defined and used for all tested configurations. In the model it was denominated as  $\Delta T_D$ . Once a droplet was generated, its new position was obtained by solving the force balance equation for constant time steps equivalent to one-fifth of  $\Delta T_D$ . The new droplet was therefore generated after the predecessor droplet(s) was/were moved five steps. The process was repeated for 100 droplets. After that, the spray pattern was obtained by plotting the trajectories (xy-plane) of all the generated droplets.

### **3.7. Droplet Charge**

The droplet's charge, expressed as a certain percentage of its Rayleigh limit, was reported by Agostinho *et al.*, (2012) to range between 5% and 10 %. However, in this model the absolute value was defined as the value which better described the spray pattern. This was the parameter which was used for fitting the spray pattern, by varying the magnitude of their dispersion. The final droplet charge at every value of applied electric potential and liquid flowrate was, therefore, used as a possible confirmation of the droplet charge in the simple-jet mode.

### **3.8. Droplet Deformation**

In the simple-jet mode at low potentials, the droplet formation happens in the varicose breakup. The droplets' random initial displacements as well as their random initial velocity vector, discussed in section 2.9, were implemented in the model, however, this could not translate into a plausible spray pattern. Instead, it was observed from the images that the droplets' deformation might be the major factor contributing to the droplet's gradual displacement from their Y- position. To verify this, a simulation of this deformation in the model was done by displacing the droplet's center of charge from its center of mass at a certain frequency (experimentally approximated). Even though it was observed that the droplets' deformation got damped with time, for simplification, a constant value of maximum displacement of the center of charge was used throughout the calculation time.

### **3.9. Validation**

The droplets' trajectories for the model were compared with the experimentally obtained trajectories. The droplets' charge, expressed as a percentage of their Rayleigh limit, was adjusted until the X-Y cross-sectional area of the spray, between the breakup point and a distance of 18mm below the breakup point, for the model and experiment agreed within 10%. The obtained adjustable percentages of the Rayleigh limit were compared with the values presented by Agostinho *et al.*, (2012), to verify their consistency.

### **3.10. Analyzing the force components**

After validating the model, various components of the force acting on a single droplet were analyzed. This was to help predict the magnitude of extra forces required to manipulate the droplets' trajectories. Various components of the different forces were analyzed for a single droplet so as to demonstrate their individual contribution. The average magnitude of these force components were then analyzed to give a clear picture about their contribution.

### **3.11. Analysis of the spray packing factor**

In order to investigate the effect of wind the spray packing factor was analyzed to determine the effect of the inter-particle interference. To achieve this, every image of the spray was resolved into two sections, (A and B), as shown in Figure 3-5.

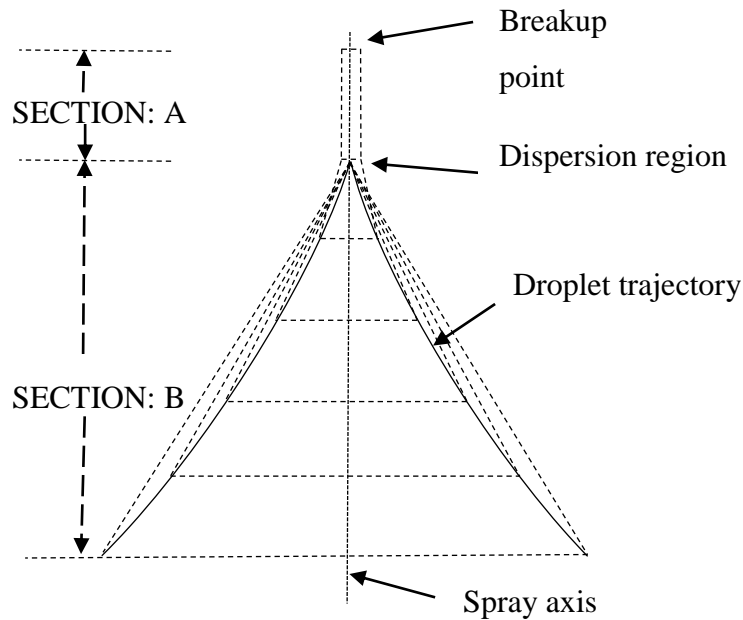


**Figure 3-5: Schematic diagram representing the spray sub-sections where the packing factor was calculated**

The dispersion region was described as the region from the breakup point where a droplet was displaced from the spray axis, for a distance more than its Feret diameter, for the first time. Section A, which extended from the breakup point to this region, was assumed to be a cylindrical in shape. The radius for this cylinder was equivalent to the displacement of the droplet, defining the dispersion region, from the spray axis, plus a half of its Feret diameter. The height for this cylinder was taken as the distance between the breakup point and the dispersion region. Section B, which extended beyond the dispersion region, was subdivided into small triangular (conical-3D) sub-sections. These sub-sections were obtained by observing the outermost droplets. The next droplet, defining a given subsection, was the one located at a distance greater than the droplet's Feret diameter (X- component) from the previous outer droplet on either side. A new triangle (cone-3D) was then introduced after this droplet. Succeeding trapezoidal volumes were approximated by subtracting the preceding conical volume from the succeeding one. Finally, the packing factor was obtained as the ratio between the effective volume occupied by all droplets within a given sub-section and the total volume of the respective sub-section. The process was repeated



for all sub-sections in a single image, and then the images superimposed to obtain a single images.

### 3.12. Investigating the effect of wind on the spray shape

In order to investigate the effect of wind on the droplets' trajectories, a laboratory experiment was set as mentioned in section 3.3, with wind introduced by a wind pump as shown in Figure 3-6.

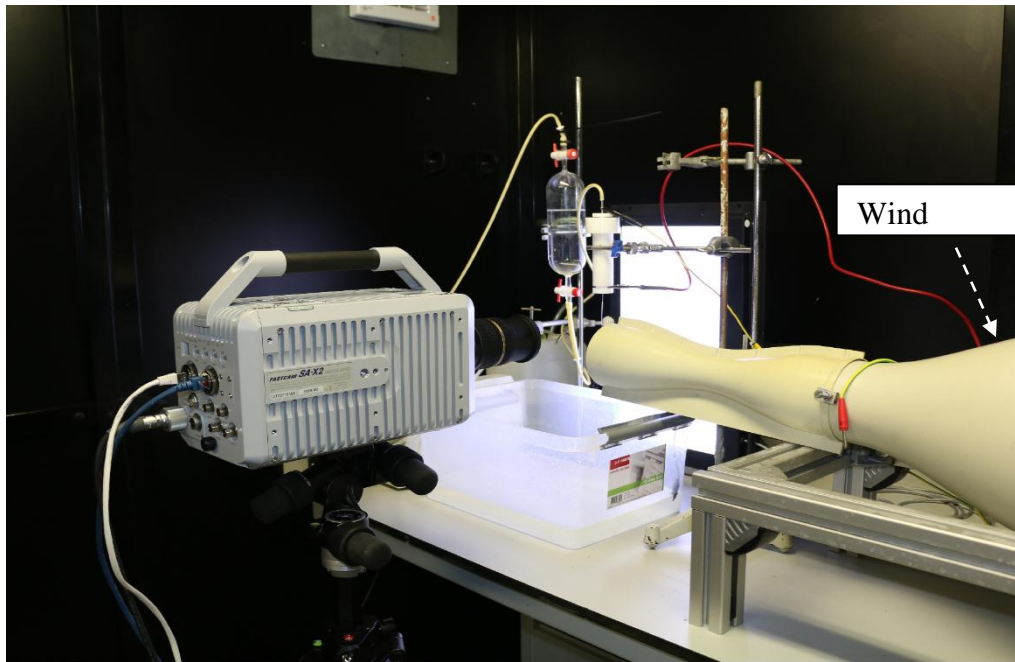


**Figure 3-6: Experimental setup for analyzing the effect of wind on the spray**

A Leybold-Heraeus pump model number 373-04 was used to blow wind through a throttling tube of 100 mm diameter. This wind was introduced perpendicular to the spray axis. The velocity of the wind was measured with a Wilh. Lambrecht KG- anemometer (measuring range between 0 and 20 m s<sup>-1</sup>).

## Chapter 4

### Results and Discussion

This section contains the results obtained for the background electric field calculation, droplets initial conditions from the experiment, simulation results for the physical model, validation of the physical model, components of force acting on the droplets, droplets packing factor and the effect of introduced air flow on the droplets' trajectories.

#### 4.1 The Calculated Background Electric Field

For the defined geometry in COMSOL Multiphysics® 4.4, the background electric field was calculated for different values of electric potential as shown in Figure 4-1

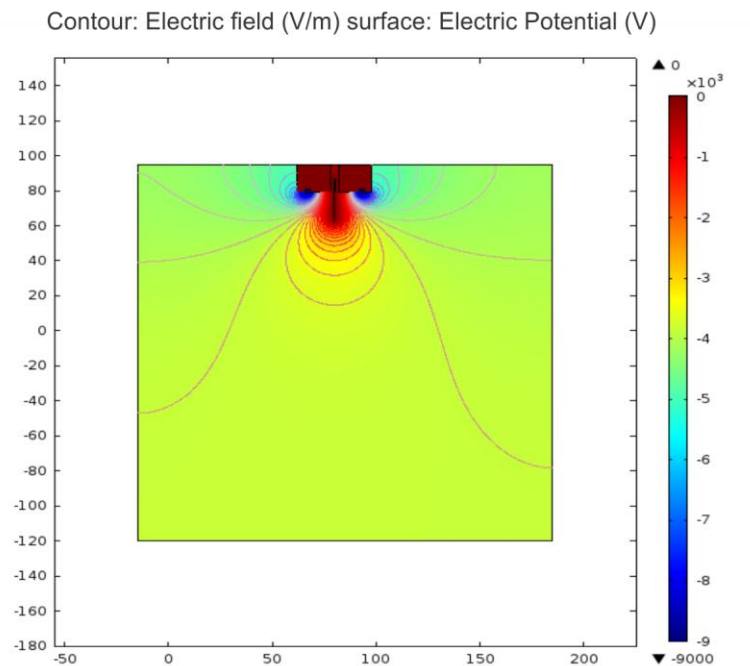


**Figure 4-1: A graph showing equipotential lines for the electric field and the surface shows the electric potential**

The graph shows that the counter-electrode ring was connected to the negative potential, while the nozzle was grounded to avoid high potential getting connected to the liquid, for safety, and at the same time produce positively charged droplets.

The field matrix was exported to MATLAB® where the X- and Y-components of the background electric field across the geometry, at the point of jet breakup, were compared

as shown in Figure 4-2. This comparison is for the flowrate of  $285 \text{ mL h}^{-1}$  and electric potential of  $-5 \text{ kV}$ .

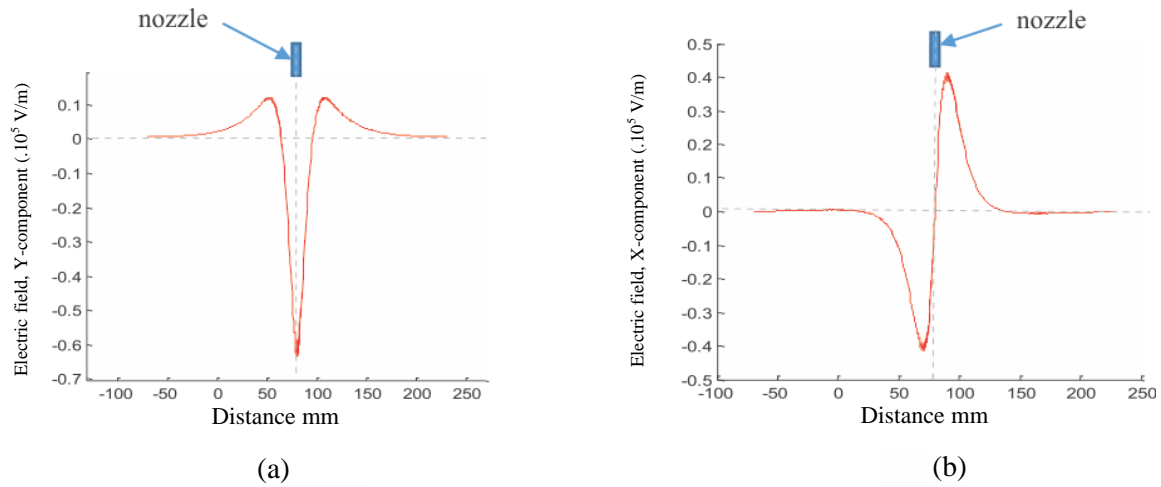


**Figure 4-2: Calculated background electric field for (a) Y-component and (b) X-component respectively**

The maximum magnitude of the background electric field for the Y-component is  $0.65 \times 10^5 \text{ V/m}$ , whereas it's  $0.4 \times 10^5 \text{ V/m}$  for the X- component. This indicates that the droplets are prone to undergo more elongation in the Y direction than in elongation the X direction near the breakup point. This phenomenon of droplets elongating parallel to an applied electric field has been reported previously by various authors (Grimm and Beauchamp, 2005). Additionally, it was found that COMSOL Multiphysics<sup>®</sup> 4.4 is a good tool that can provide detailed information about the background electric field force component at each position on the xy-plane for the studied geometry. Even though practical comparisons were not performed in this work, it is believed that such a tool might considerably decrease the total computational time of the model.

## 4.2 Experimental results and model input parameters

Figure 4-3 ( a to c) presented below shows the values obtained for the characterization of the droplets average Feret diameter, the jet breakup length and the droplets' initial velocity for all the investigated EHDA settings.

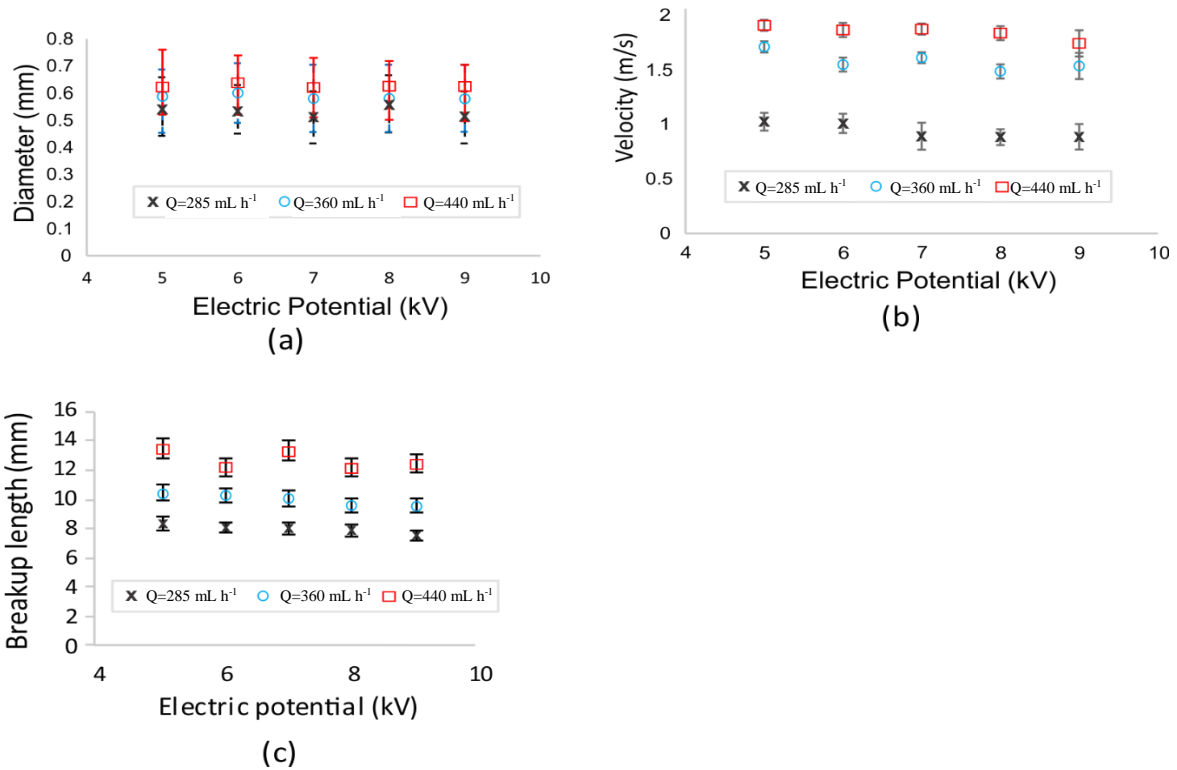


**Figure 4-3: Experimental results for different values of liquid flowrate and applied electric potential; (a) the droplets' average Feret diameter, (b) the droplets' initial velocity, and (c) the jet breakup length. In all cases, the error bars represent the standard deviation, in Figure 14a and Figure 14b, and in Figure 14c it is the percentage error of 10% for each measurement.**

As it can be seen in Figure 4-3 (a), the droplets' average Feret diameter increases with increase in liquid flow rate, while it doesn't vary significantly with the applied electric potential. This is consistent with the data presented by Agostinho (2013). A direct conclusion is that the liquid flow rate is the dominant parameter that determines the droplets' size in this mode. Therefore, for this physical model, the average droplet diameter was taken as 0.53 mm, 0.58 mm and 0.62 mm respectively for 285 mL h<sup>-1</sup>, 360 mL h<sup>-1</sup> and 440 mL h<sup>-1</sup>. The results obtained from the investigation of the droplets' initial velocity are shown in Figure 4-3 (b). From here, it can be shown that the droplets' initial velocity increases with increase in liquid flowrate, but it is slightly affected by the applied electric potential. For simplification, the value of 1.05 m s<sup>-1</sup>, 1.6 m s<sup>-1</sup> and 1.95 m s<sup>-1</sup> were used for the flowrates of 285 mL h<sup>-1</sup>, 360 mL h<sup>-1</sup> and 440 mL h<sup>-1</sup> respectively.

The results of the jet breakup length measurements show that the jet breakup length increases with increase in the liquid flowrate, while it slightly decreases with increase in electric potential (Figure 4-3c). This is also in accordance with Agostinho (2013). In the physical model, for simplification, the breakup length was assumed constant and equal to 8.0 mm, 10.0 mm and 12.0 mm for the flowrates of 285 mL h<sup>-1</sup>, 360 mL h<sup>-1</sup> and 440 mL h<sup>-1</sup> respectively.

The experimental droplets' size distribution for the primary droplets was analyzed for the tested applied electric potentials and liquid flowrates. In all the analysis, the total population of the droplets ranged between 250 and 400, every droplet being considered for about 20 times, depending on the number of times the droplet appeared within the window, which was focused by the camera. These distributions are shown together with the simulated droplet size distribution in Figure 4-4.

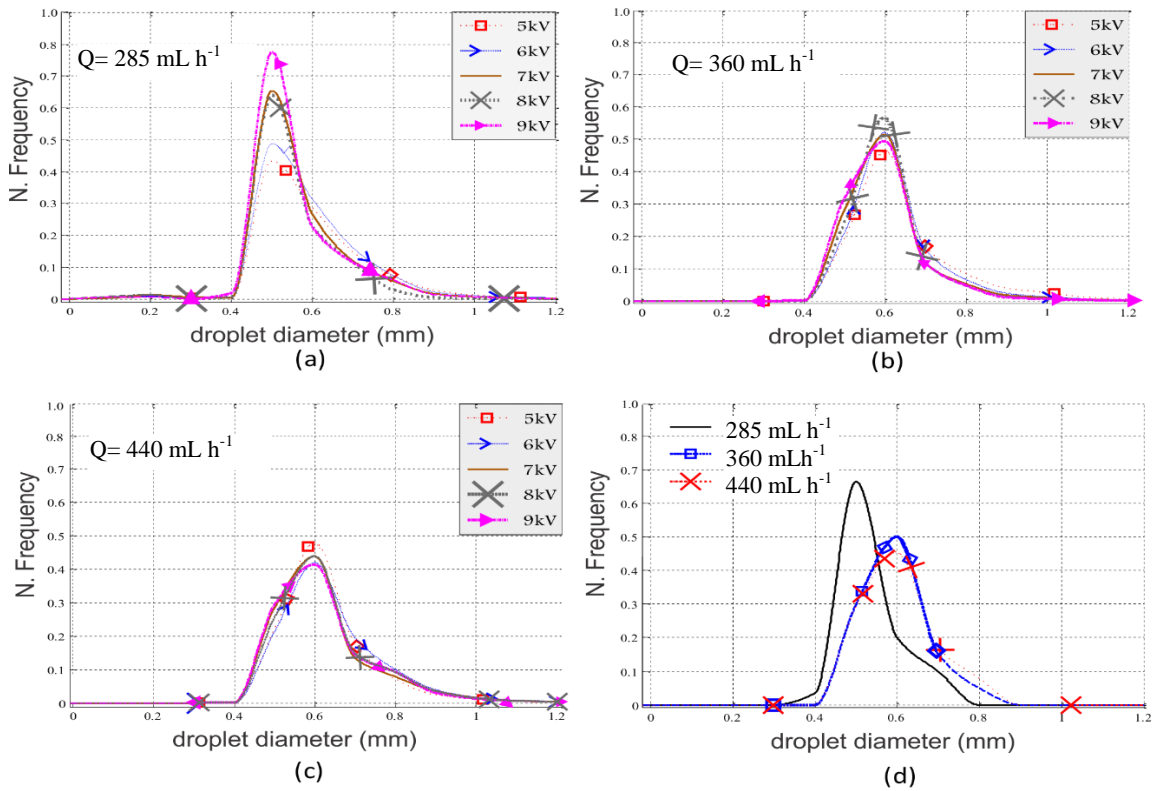


**Figure 4-4: Droplets' size distribution for potentials ranging between -5 kV and -9 kV at the flow rates of (a) 285 mL h<sup>-1</sup> (b) 360 mL h<sup>-1</sup>, (c) 440 mL h<sup>-1</sup> for experimental data and (d) for simulated size distribution**

The calculated droplets' relative standard deviation (RSD) was found to range between 0.166 and 0.214. According to Agostinho (2013), an  $RSD < 0.2$  can be considered to indicate a monodisperse size distribution.

### 4.3 Droplet Deformation

Figure 4-5 shows a section of an intact jet length and some droplets breaking up from the jet.

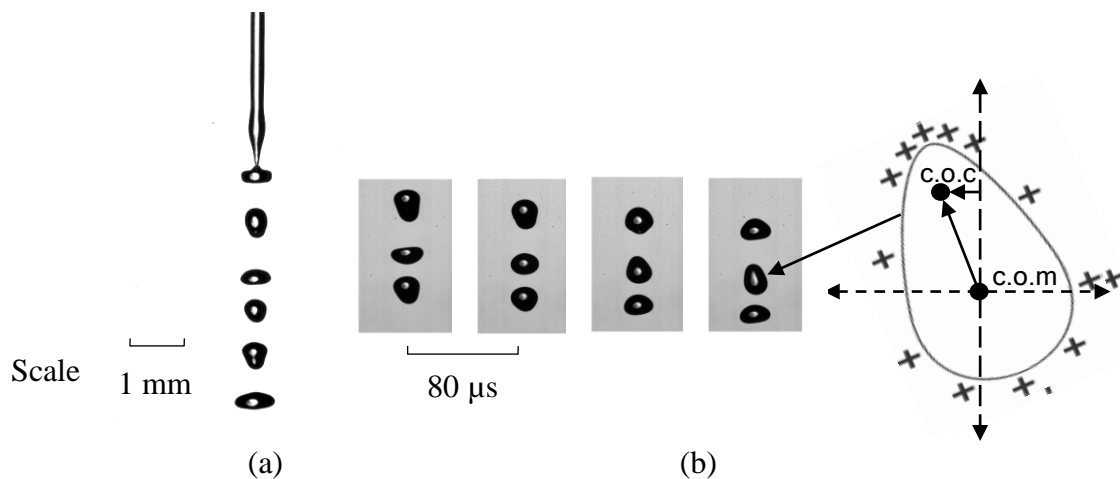


**Figure 4-5: A demonstration of charge displacement by images taken by a high-speed camera at a speed rate of  $12500 f_{ps}$ ; (a) A Section of an intact length, with droplets undergoing deformation after they breakup from the jet, (b) evolution of three droplets in four steps after they breakup from the jet, and (c) displacement of the center of charge (c.o.c) from the center of mass (c.o.m).**

From here, it is clear that the droplets are undergoing deformation after breakup, it can also be seen that the droplets undergo deformation at a certain periodic sequence. Further, the deformation is larger in the Y- direction than in the X- direction. This droplet deformation causes a non-uniform charge distribution on its surface, and this causes the displacement of its center of charge from its center of mass (Fricker, 1989; David *et al.*, 1997) (Figure 4-5 c). Since all the electric forces acting on the droplet are considered to be concentrated at the center of charge, the droplet will experience a substantial amount of X-component of force, which will initiate the dispersion and directly influence the spray pattern.

#### 4.4 Simulated Droplets' Deformation

To implement these droplets' deformation in the model, their centers of charge were harmonically displaced from their centers of mass (Figure 4-5b), in the Y and X directions. For simplification, the droplets were assumed to be perfect conducting spheres. This assumption proves to be right, because the charge relaxation time (Equation. 4.1) (Hartman, 1998) for the droplets is much smaller than the droplets' period of deformation, which ranges between 480  $\mu\text{s}$  and 641  $\mu\text{s}$  (derived from the observed deformation frequency).

$$\tau = \frac{\epsilon_0 \epsilon_r}{K} \dots \dots \dots \text{Equation 4.1}$$

In order to find values which could realistically translate the displacements of the droplet's two centers and test the proposed theory, a fitting procedure was defined in the following way. Firstly, the behavior of the sprays droplets was observed for different flowrates and applied electric potential. From these experiments it could be concluded that the produced droplets undergo shape deformation after breakup in a harmonic pattern, i.e. 1560 Hz (for 440  $\text{mL h}^{-1}$  and 360  $\text{mL h}^{-1}$ ) and 2080 Hz (for 285  $\text{mL h}^{-1}$ ). After this analysis a specific spray configuration was chosen (285  $\text{mL h}^{-1}$  and 5 kV) to be tested in the model. In this test, a displacement of the droplets center was brought to the model at a defined frequency (2080Hz) with different magnitudes for the horizontal and the vertical displacement. For every tested magnitude, the spray dispersion obtained in the model was compared to images taken from experiments using the same flowrate and potential. Two important conclusions were obtained from this first check, namely: (i) the best fit between models and experimental images was obtained when the maximum displacement between the droplets' centers was 60% in the vertical direction and 30% in the horizontal direction (Figure 4-6). (ii) When the procedure was repeated for other flowrates and electric potentials, the results showed that these maximum values of displacement remain the same.

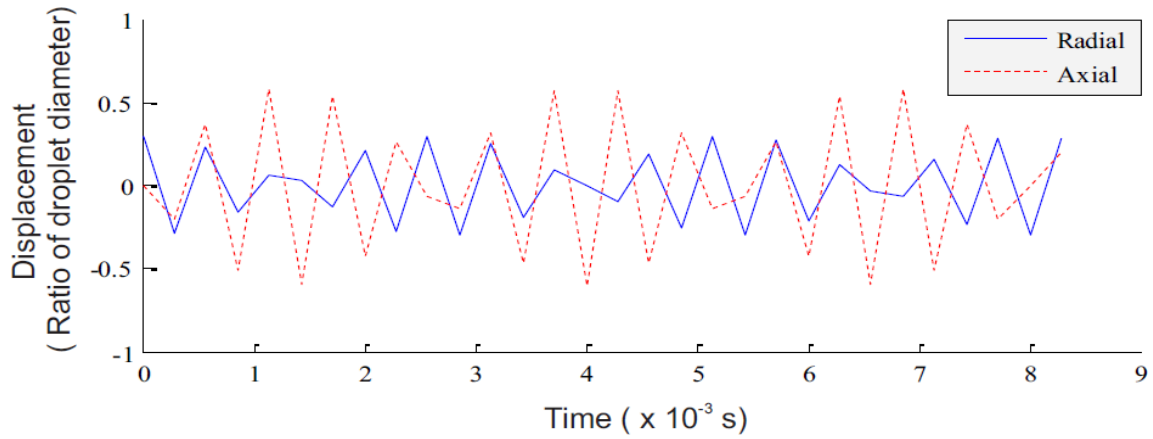


**Figure 4-6: Displacement of the center of charge in the X and Y directions due to droplet’s deformation**

During the tests, the observed fact that the droplets deformation was getting damped as they moved away from the break-up point was neglected.

#### 4.5 Experimental Droplets’ Trajectories

Figure 4-7 (a) is a representation of a single spray image and Figure 4-7 (b), is a representation of the droplets trajectories after isolation from the images by a MATLAB<sup>®</sup> routine. The routine isolated the individual droplets from the images taken by a high speed camera and traced their individual trajectories. The spray starts in the Y axis from the breakup point, and it’s symmetrically presented in the X-axis i.e., nozzle axis. The routine was used to obtain the droplet's velocity, as well as the spray patterns, for different values of the applied electric potential and liquid flowrate, which were used for validating the model.



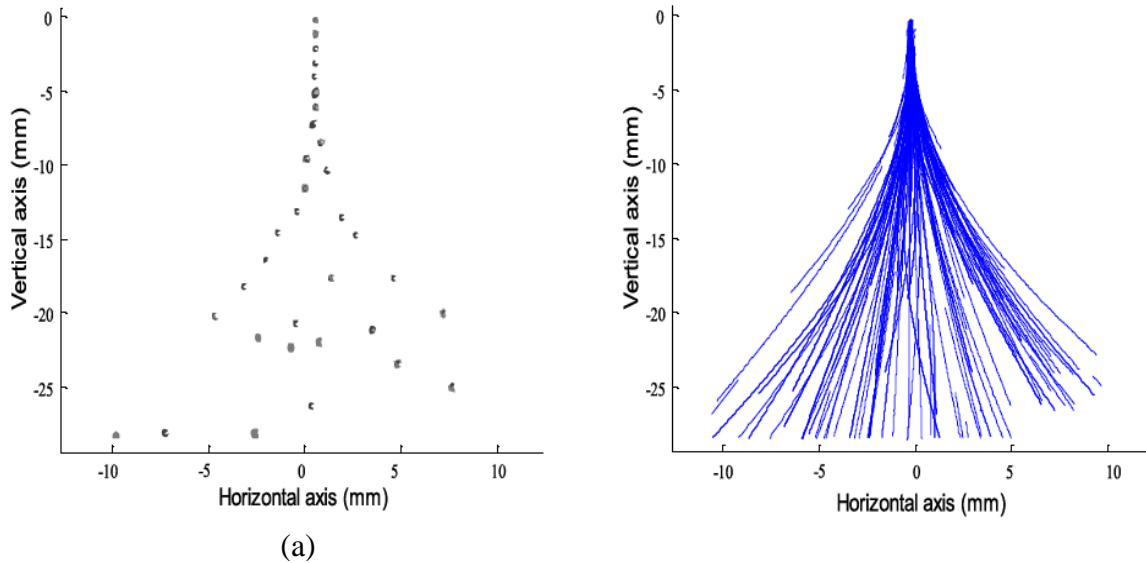


**Figure 4-7: Isolation of individual droplets from the images to obtain the experimental droplets' trajectories: (a) a single image of the spray; (b) Experimental droplets' trajectories**

This developed routine was, therefore, used to isolate the individual droplets and obtain the experimental spray shapes used to validate the theoretical shapes in the next section.

#### **4.6 General spray shape for the calculated droplets' trajectories**

Figure 4-8 show the general theoretical spray shape for different values of the applied electric potential and liquid flowrate.

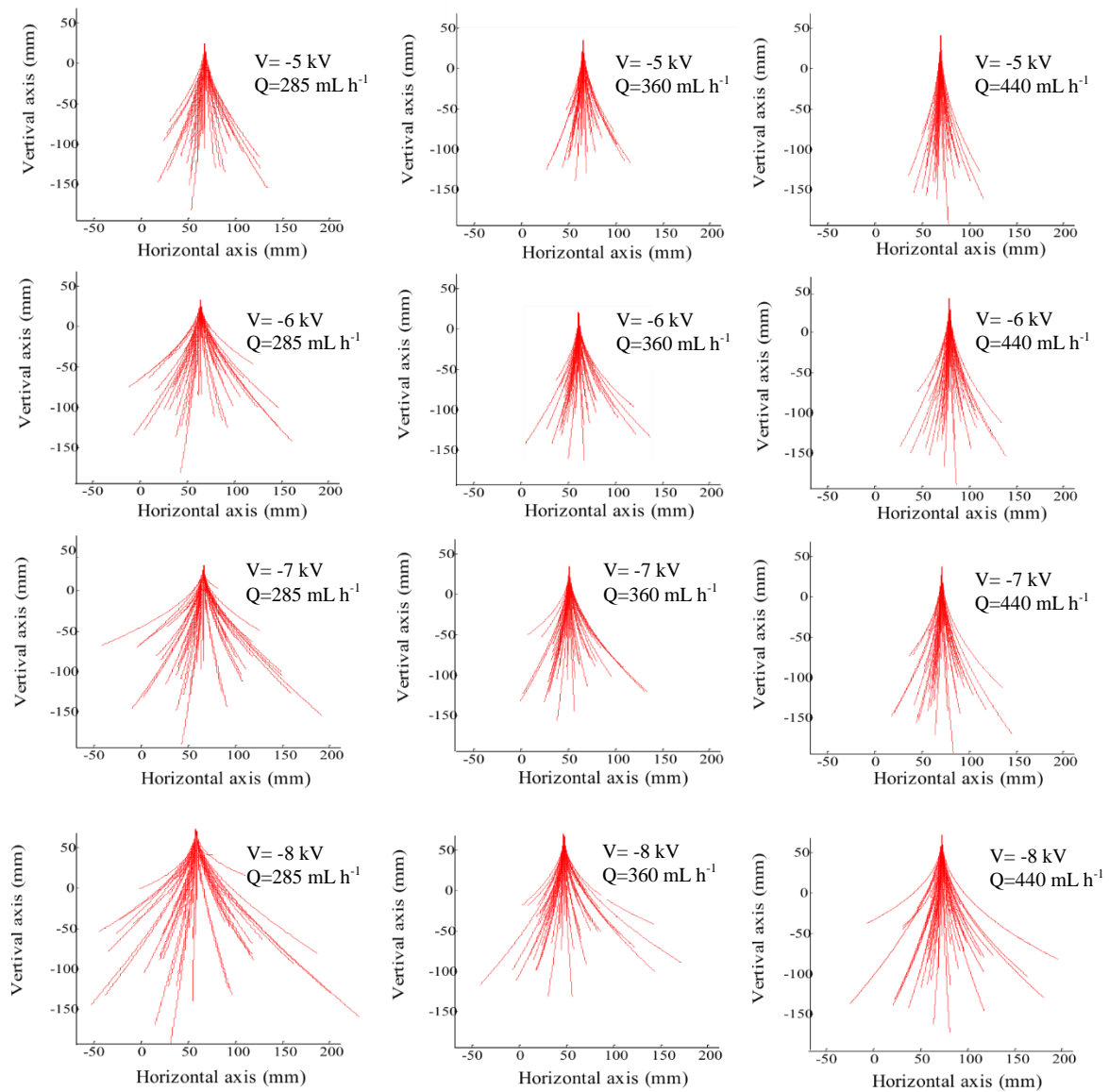


**Figure 4-8: General spray shape for the calculated droplets' trajectories at different values of applied electric potential at liquid flowrates**

It can be seen from the figure that the spray dispersion widens with increase in electric potential, while it decreases with increase in the liquid flow rate.

A more qualitative analysis on the similarities between the experimental and theoretical sprays was done by comparing the spray patterns. The spray shapes for the experimental and the calculated droplets' trajectories are shown in Figure 4-9. For simplified presentation of the validated results, only the external droplets' trajectories were used to compare the theoretical spray shapes with their corresponding experimental spray shapes.

These trajectories were defined using CorelDRAW<sup>®</sup> X7. The results are shown in Figure 4-9.

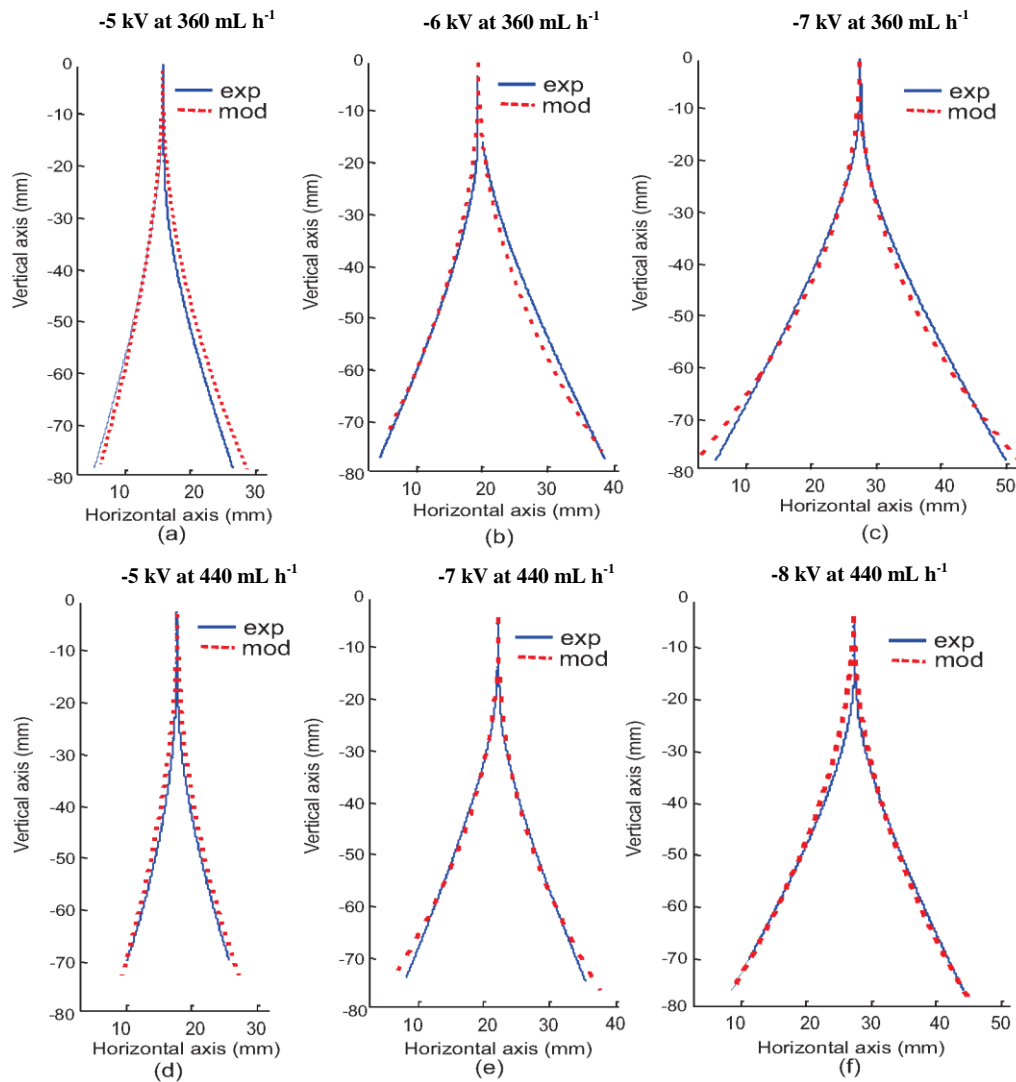


**Figure 4-9: Experimental and theoretical droplets' trajectories for some values of the applied electric potential and liquid flowrate**

From Figure 4-9 the model describes the spray pattern, comparably, for the shown parameters, as well as for the other values of liquid flowrate and applied electric potential. Additionally, a quantitative analysis was done by approximating the spray areas to triangles and comparing them. The triangles had their apex located at the breakup point and the bases located at some distance from the breakup point as shown in Figure 4-10.



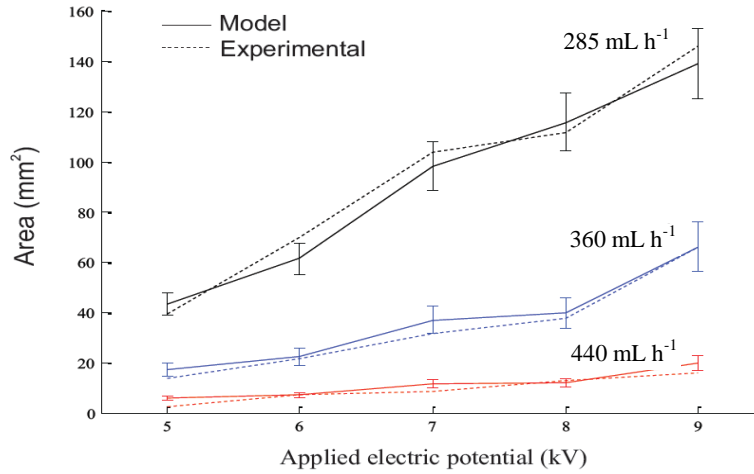


**Figure 4-11: Y- cross-sectional area of the electro spray, between the breakup point and a distance of 18 mm from the breakup point for electric potential ranging between -5 kV and -9 kV with the flow rates of 285 mL h<sup>-1</sup>, 360 mL h<sup>-1</sup> and 440 mL h<sup>-1</sup>**

The plot shows good agreement between the areas of the real and modelled spray shapes within an error of 10%. It also shows that the area decreases with increase in liquid flowrate and increases with increase in applied electric potential.

#### 4.7 Droplet Charge

The plot presented in Figure 4-12 shows the final values of the adjusted droplet charge, and their corresponding percentage of the Rayleigh Limit for the tested configuration. These were the values that described the spray shapes best, for different setting of liquid flowrate and applied electric potential.

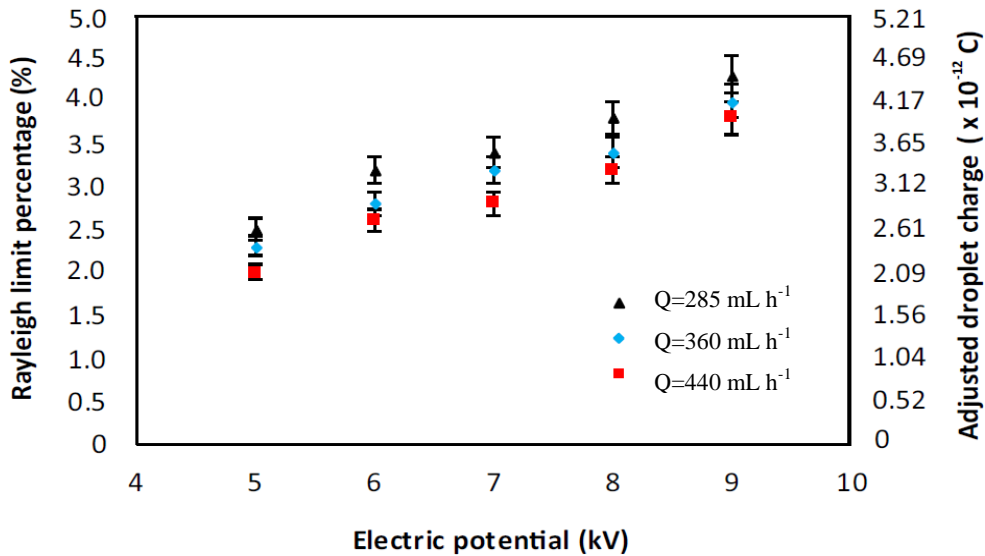


**Figure 4-12: Simulated droplet charge as a percentage of its Rayleigh limit**

The droplets' charge increases with increase in the applied electric potential, and decreases with increase in the liquid flowrate. It ranges between 2.0% and 4.5% of the droplets Rayleigh limit, for the tested values of liquid flowrate and applied electric potential.

#### 4.8 Velocity Profile

Figure 4-13 shows the x component of velocity of the droplets near the breakup point for the experimental and model analysis.

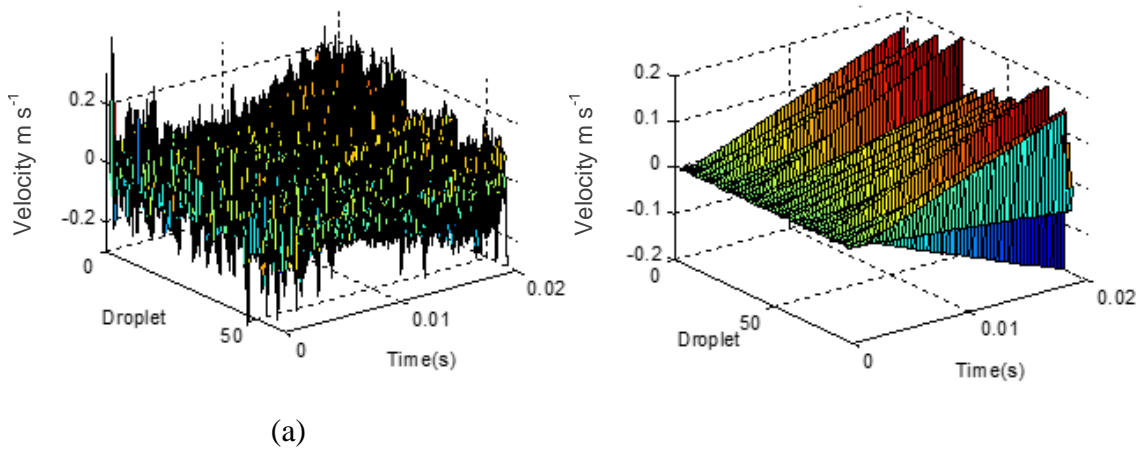


**Figure 4-13: The X-component velocity of droplets at an applied electric potential of -5 kV and liquid flowrate of 285 mL h<sup>-1</sup>; (a) experimental and (b) theoretical.**

It is observed that this component of velocity increases steadily (in both directions from the y-axis) with time for both the experimental and the modelled droplets. However, the variation of this value near the breakup point is high for the experimental results in Figure 4-14a. After stabilization this velocity is observed to rise steadily with time, just like in the case of the calculated values in Figure 4-14b. This is expected because the droplets undergo high deformation near the breakup point and additionally, they continue to accelerate until they attain the settling velocity.

Figure 4-14 shows the droplets' y-component of velocity for the experimental and calculated results respectively.

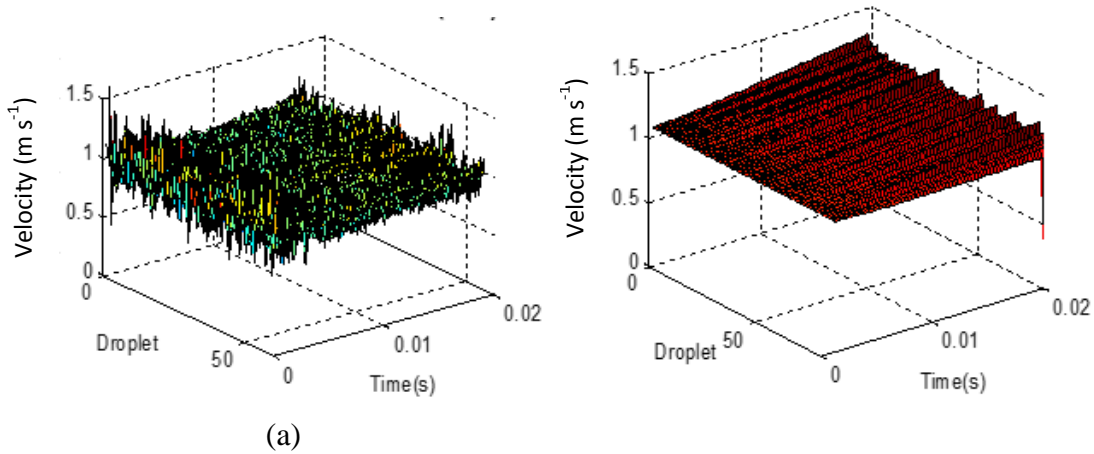


**Figure 4-14: The Y-component velocity of droplets at an applied electric potential of - 5 kV and liquid flowrate of 285 mL h<sup>-1</sup>; (a) experimental and (b) theoretical.**

It can be seen that for the experimental results the velocity exhibits high variation. This is because the droplets undergo high deformation immediately after breakup and therefore the center of mass highly varies causing this variation of velocity. Once the droplets move further from the breakup point, their deformation is damped and their velocity becomes almost stable. It can be observed further that the droplets' velocity increases steadily with time for both the experimental and the calculated values.

### 4.9 Force components

Figure 4-15 shows a 3-dimensional representation of the X- and Y-components of the background electric field respectively.

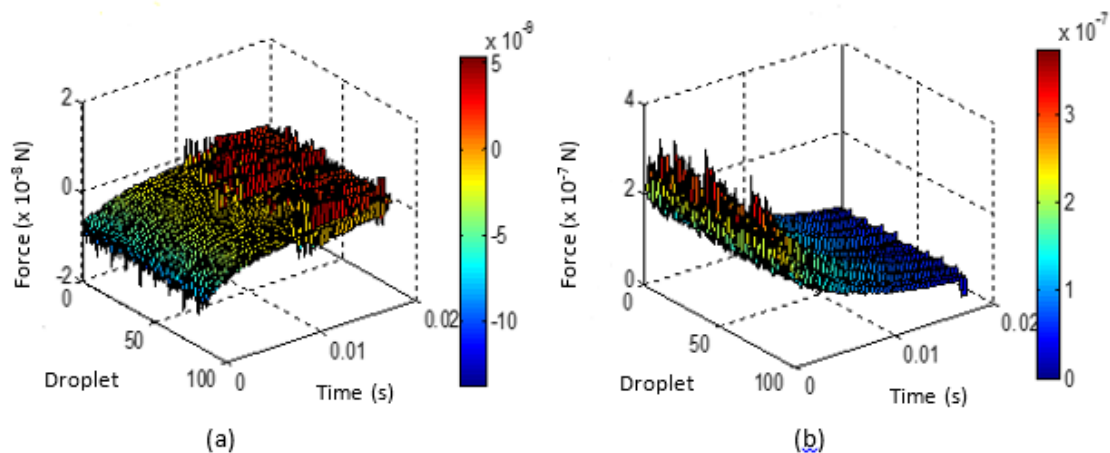


**Figure 4-15: The calculated background electric field force acting on the droplets as they break up from the jet; (a) the X-component and (b) the Y-component**

The x-axis represents the droplets from the first one to the  $N^{\text{th}}$ , where  $N$  is the total number of droplets considered. The y-axis represents time in seconds (from 0 to  $20 \times 10^{-3}$  s). The z-axis represents force (N). The legend shows the variation of this force with time for all the droplets.

It can be seen from the Figure 4-15 that the Y-component of force decreases rapidly from  $0.22 \mu\text{N}$  to  $0.04 \mu\text{N}$  within a duration of 20ms as the droplets move away from the breakup point. For the X- component, this value changes from  $0.007 \mu\text{N}$  to  $0.002 \mu\text{N}$ .

Figure 4-16 shows the inter-droplet coulombic force between charged droplets, for X and Y-components respectively.

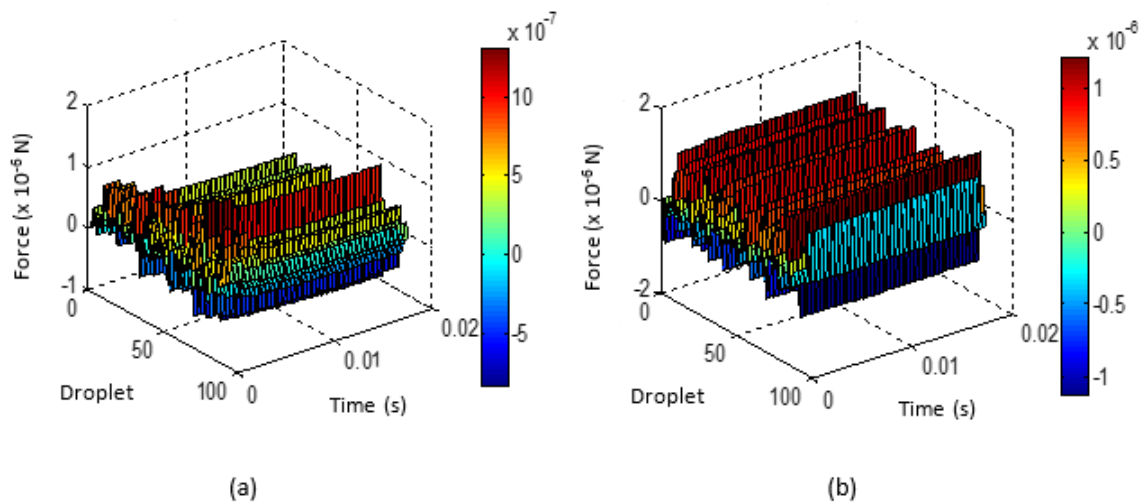


**Figure 4-16: The calculated inter-droplet coulombic force acting on charged droplets as they move away from the breakup point; (a) the Y-component and (b) the X-component**

This force is almost constant for each droplet, exhibiting some abrupt changes after which it remains constant again. This value depends on the region where the droplet is positioned with respect to other droplets. At the spray center, the forces acting on the droplet from different sides oppose each other to decrease the value of the resultant force. Droplets existing towards the periphery of the spray, experience more resultant force.

The Figure 4-17 shows the drag force for x and y components respectively.



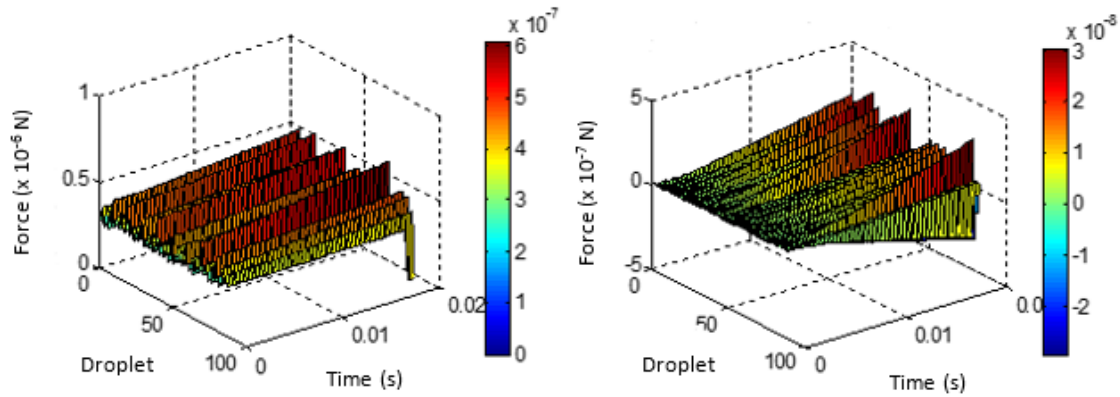


**Figure 4-17: The calculated drag force of interaction acting on individual droplets as they move away from the breakup point; (a) the Y-component and (b) the X-component**

It can be seen from the Figure 4-17 that the resolved Y-component of the drag force is higher than the X-component. This can be attributed to the difference in the droplet's velocity. However, both of them are steadily increasing with time indicating the droplets' acceleration.

#### 4.10 Representation of forces acting on the droplet

Figure 4-18 shows different forces, decomposed in X and Y components, acting on a single droplet of 0.741 mm, for an applied electric potential of 5 kV and a flowrate of 360 mL h<sup>-1</sup>.

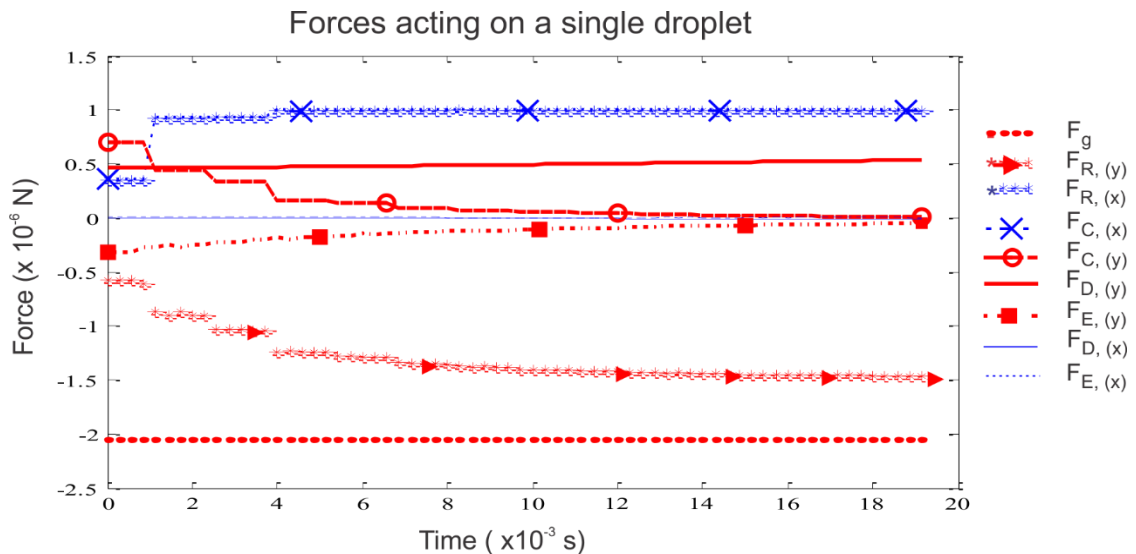


**Figure 4-18: A representation of all force components acting on a single droplet within a duration of 20 ms after its generation.**

The X-component of the background electric field force,  $\vec{F}_{E(x)}$ , is quite small as compared with the Y-component,  $\vec{F}_{E(y)}$ , which decreases as the droplets move away from the breakup point. The X-component of the inter-droplet coulombic force,  $\vec{F}_{C(x)}$ , is much higher than the Y- component,  $\vec{F}_{C(y)}$ , and it almost contributes solely to the resultant force, in the X-component,  $\vec{F}_{R(x)}$ . After decomposing the drag force, the Y-component of the drag force,  $\vec{F}_{D(y)}$ , proves to be much higher than the X- component,  $\vec{F}_{D(x)}$ . This is due to the higher component of velocity in the Y- direction than in the X- direction.

Figure 4-19 shows the average magnitude of all force components acting on all the droplets for different values of applied electric potential at a flowrate of 285 mL h<sup>-1</sup>.

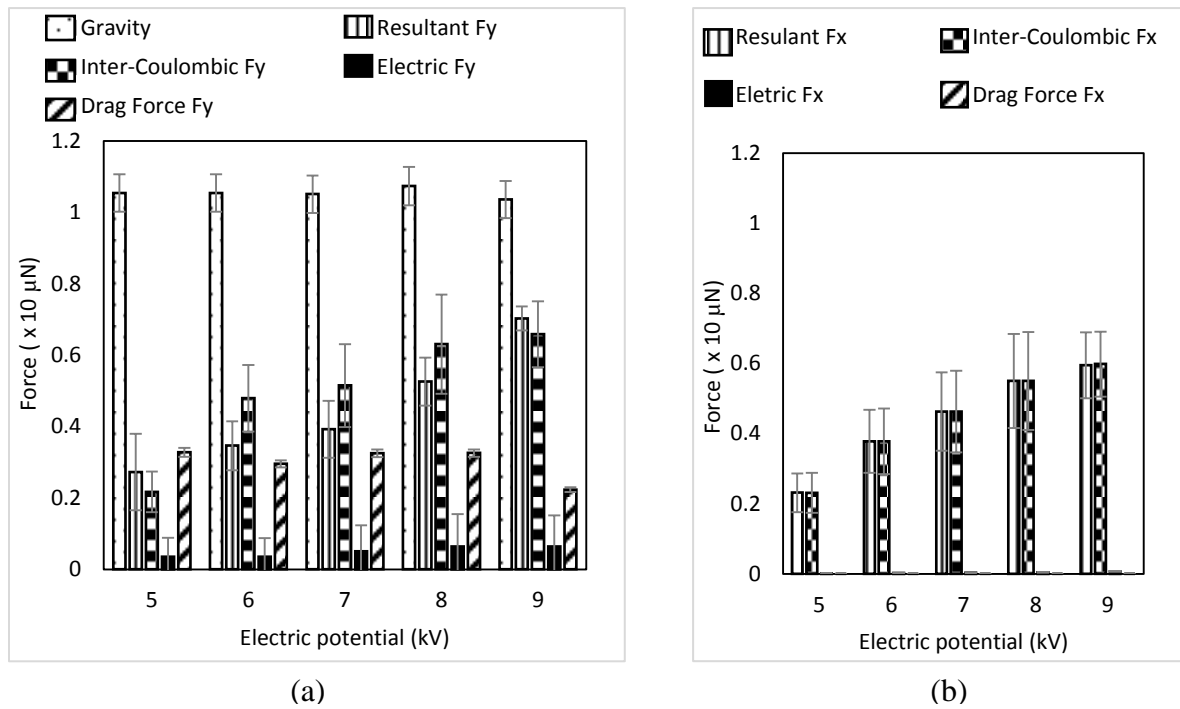


**Figure 4-19: A representation of the average magnitude of various force components acting on all the individual droplets within a duration of 20 ms after their generation; (a) Y- component, (b) X- component. The error bars represent the standard deviation**

The analysis of the average magnitude of the forces acting on the droplets shows that the gravitational force,  $\vec{F}_g$  has the highest average magnitude, and the inter-droplet coulombic force,  $\vec{F}_{C(x,y)}$ , plays a major role in dispersing the droplets as compared to the background electric field force,  $\vec{F}_{E(x,y)}$ . It is, therefore, not realistic to manipulate the droplets'

trajectories by using a secondary background electric field, without interfering with the droplets' formation. This is because a very strong background electric field, about  $0.224 \times 10^6$  V/m (an applied electric potential of about 67.2 kV across the defined window of 300 mm by 300 mm), is required to overcome the force of gravity, which is the most dominant force.

#### 4.11 Droplets' packing factor

The change of the droplets' packing factor with distance from the breakup point for the flowrate of  $285 \text{ mL h}^{-1}$ ,  $360 \text{ mL h}^{-1}$  and  $440 \text{ mL h}^{-1}$  at an applied electric potential of -6 kV is represented in Figure 4-20 respectively. A total number of 1300 images were analyzed in each case. The analysis was done and then the images were superimposed to form one image. Each dot on the graph indicates the calculated value of the packing factor at a given distance from the breakup point.

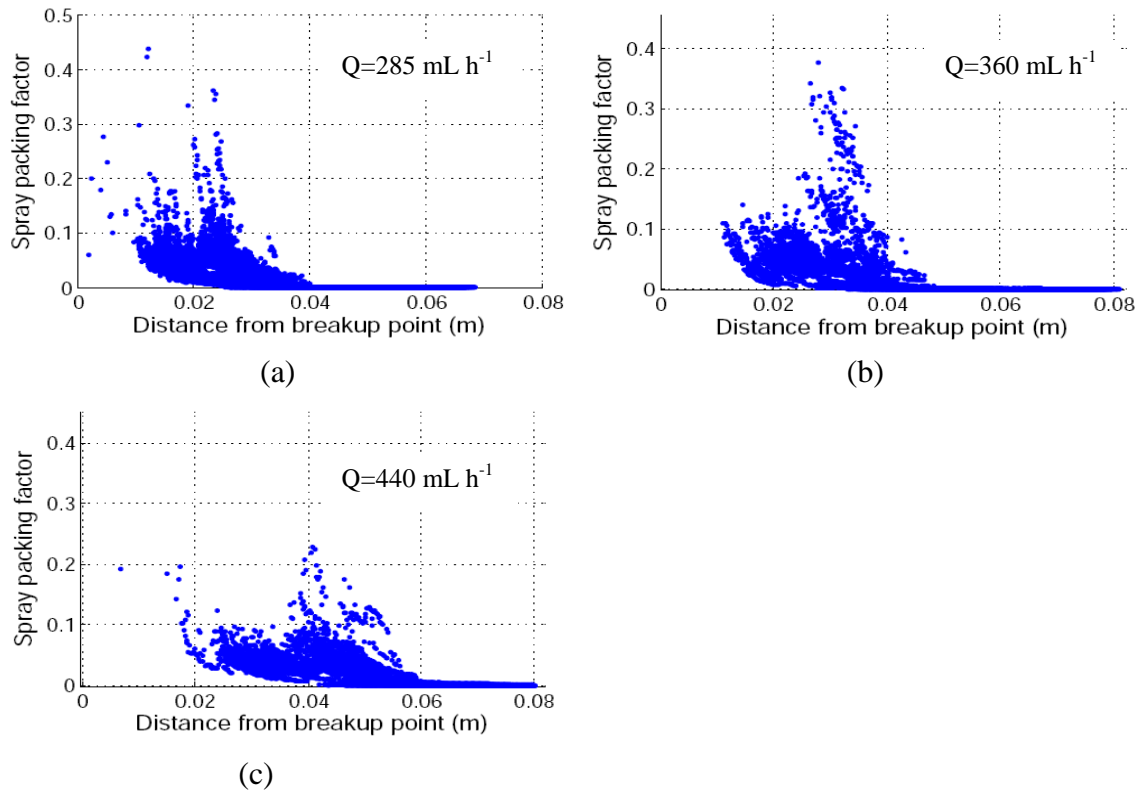


**Figure 4-20: Graphs showing the variation of the droplets packing factor with distance from the breakup point at an applied electric potential of -6 kV and for different liquid flowrates; (a)  $Q= 285 \text{ mL h}^{-1}$ , (b)  $Q= 360 \text{ mL h}^{-1}$ , (c)  $Q= 440 \text{ mL h}^{-1}$ .**

It can be seen that the droplets' packing factor decreases rapidly with increase in distance from the breakup point. The packing factor decreases faster at lower flowrate as compared to higher flowrate. For the flowrate of  $285 \text{ mL h}^{-1}$ , the packing factor is less than 0.02 at a distance of 40 mm from the breakup point, and then at 50 mm and 60 mm, for the flowrate of  $360 \text{ mL h}^{-1}$  and  $440 \text{ mL h}^{-1}$  respectively.

#### 4.12 The effect of wind on the droplets' trajectories

The application of a uniform wind velocity field was investigated experimentally as well as theoretically in the model as shown in Figure 4-21. In both cases, wind of uniform velocity field was applied perpendicularly to the nozzle axis, at a distance of 40 mm from the breakup point.

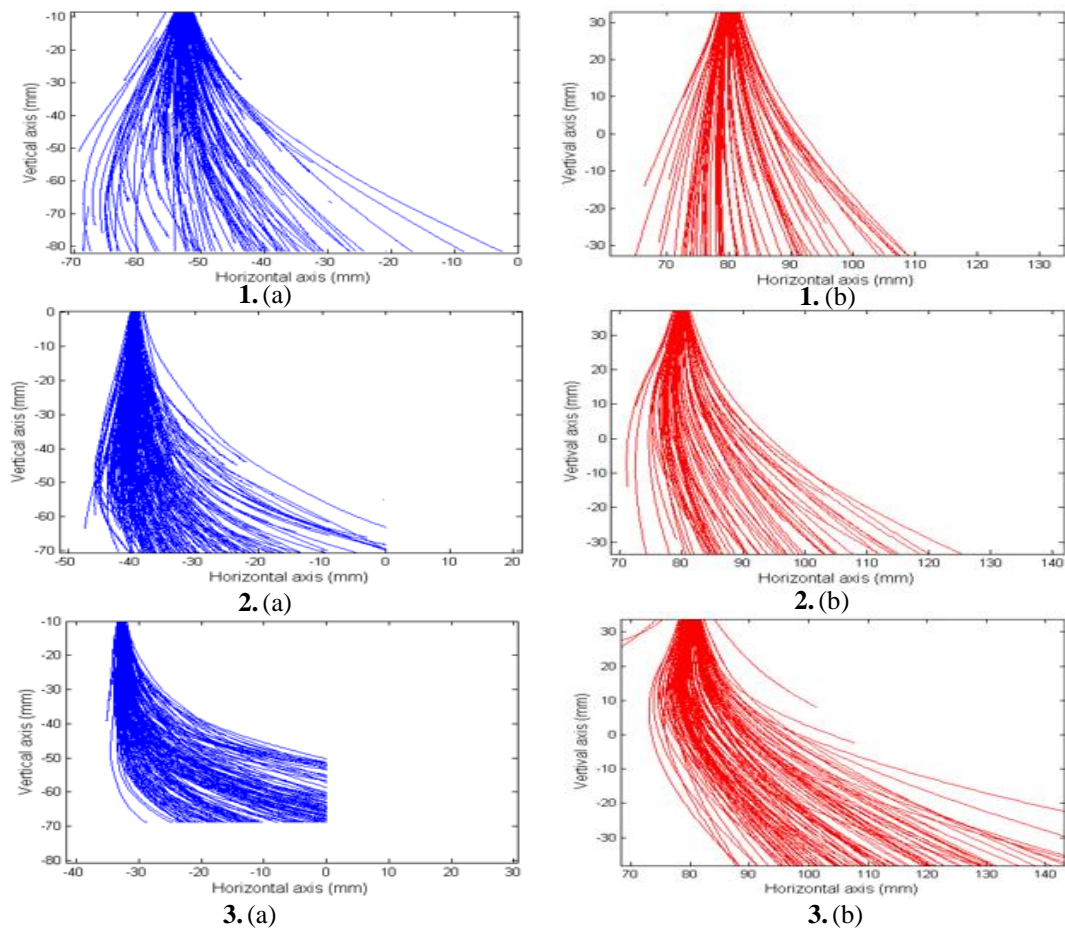


**Figure 4-21: Droplets' trajectories for the flowrate of  $285 \text{ mL h}^{-1}$  and an applied electric potential of  $-6 \text{ kV}$  with an introduced wind; (a) Experimental results and (b) theoretical results, for different values of velocity; (1)  $2 \text{ m s}^{-1}$ , (2)  $4 \text{ m s}^{-1}$ , and (3)  $6 \text{ m s}^{-1}$**

It can be seen that the introduction of an air flow in the model causes the same deflection to the spray, just as in the experimental scenario. It is therefore concluded that an introduction of a uniform velocity field to the model is realistic. The droplets are well spaced apart, such that the velocity field of the air flow remains fairly uniform.

## Chapter 5

### Conclusion and Recommendations

#### 5.1 Conclusion

The presented model for describing the droplets' trajectories in the simple-jet mode of electro spraying is validated. This model can provide the design pre-parameters for those systems that depend on electro spraying at high throughput. It also introduces the possibility of investigating the effect of additional forces on the spray.

From this model, the mechanism in which the droplets' dispersion is initiated was disclosed as the droplets' deformation. This is due to the displacement of the droplet's center of charge from its center of mass. Further, the droplets' charge was found to range between 2% and 4.5% of their Rayleigh limit. This is comparably consistent with the values which were reported by Agostinho *et al.*, (2012). The authors reported values ranging between 5% and 10% of the droplets' Rayleigh limit.

This model develops an insight about the relative importance of various components of forces acting on the droplets to determine their trajectories. It provides the possibility to decide on the extra forces necessary to manipulate the droplets' trajectories. Additionally, it is confirmed that the role of the background electric field is insignificant in dispersing the droplets, and therefore, it's not recommendable to use a secondary background electric field to manipulate these droplets' trajectories.

The experimental results confirm that the liquid flowrate is a more dominant factor than the applied electric potential in determining the droplets' average diameter, droplets' size distribution, jet breakup length, and the droplets' initial velocity. This is because the mechanism of droplet formation is highly dependent on the liquid flowrate as compared to the applied electric potential.

It was observed that the droplets' packing factor decreases rapidly with distance from the breakup point. It is, therefore, realistic to introduce an airflow on the spray, to manipulate the droplets' trajectories in the model, by neglecting the inter-particle interference (uniform velocity field) in the region where the packing factor was less than 0.02. Here the droplets are well spaced, and therefore the velocity field is uniform. This effect of wind on the

droplets' trajectories can be evidenced at a velocity of as low as  $2 \text{ m s}^{-1}$  and it rapidly increases for the value of  $6 \text{ m s}^{-1}$ . Therefore, an airflow is recommended for the manipulation of the droplets' trajectories.

## **5.2 Recommendations**

Despite the fact that various phenomena have been disclosed about the Simple-jet mode of electrospray in this work, the following recommendations have been given.

- 1) Further research needs to be carried out, separately, to determine the exact location of the center of charge in a deformed droplet.
- 2) Separate experiments need to be carried out to determine the exact charge on the droplets. This can be carried out by measuring the amount of current consumed in the spray using a very high precision instrument, because the amount of current drawn is in the range of nano-Amperes.
- 3) The 2D approach gave good agreement with the used validation technique (imaging technique). However, it is expected that a 3D approach would provide a more complete image of the droplet trajectories and final spray. Future experiments have thus to be performed both implementing a 3D environment to the model itself and to implement a 3D validation technique.

By extensively covering these areas, there will be improved understanding on the simple-jet mode of electrospray. This will result into more effective application of this mode in various industrial sectors.

## References

Agostinho, L. (2013). Electrohydrodynamic Atomization in the Simple-Jet Mode. Phd Thesis, Delft University of Technology, Netherlands

Agostinho, L. et al., (2012). Morphology of water Electrospays in the Simple-jet mode. *Physical Reviews E*, 066 (86) 317-326

Ashgriz, N. and Yarin, L. (2011). *Capillary Instability of Free Liquid Jets*, New York: Springer.

Bhattacharya, K. (2010). *Scope of Center of Charge in Electrostatics*, Mumbai: Tata Institute of Fundamental Research

Cloupeau, M. and Prunet-Foch, B. (1990). Electrostatic spraying of liquids: main functioning modes. *Journal of Electrostatics* 25 165-184

Cloupeau, M. and Prunet-Foch, B. (1994). Electrohydrodynamic spraying functioning modes: a critical review. *Journal of Aerosol Science* 25 (6) 1021-1036

Corson, L. et al., (2014). Deformation of a nearly Hemispherical Conducting Drop due to an Electric Field: Theory and experiment. *Physics of fluids* [online] 26 (6) 122106. Available from <<https://doi.org/10.1063/1.4903223>> [10 April 2017]

David, H., Robert, R. and Jearl, W. (1997). *Fundamentals of Physics*. New York: John Wiley & Sons, Inc.

Fricker, H. (1989). Why does charge concentrate on points?' *Phys. Educ. United Kingdom* 24 157-161

Fuchs, N. (1964). *The mechanics of Aerosols*. Toronto: Pergamon Press Ltd.

Gañán-Calvo, A., Lasheras, J., Davila, J. and Barrero, A. (1994). The electrostatic spray emitted from an electrified conical meniscus. *Journal of Aerosol Science* 25 1121-1142

Geerse, K. (2003). *Applications of Electrospay; from people to plants*. Phd Thesis, Delft University of Technology, Netherlands

Gilbert, W. (1600). *De Magnete*. London: Peter Short

Gomez, A. and Tang, K. (1994c). Electrospay of Monodispersed Water Droplets for Targeted Drug Inhalation. *Journal of Aerosol Science* 25 (6) 1237-1249



- Grace, J. and Dunn, P. (1996). Droplet Motion in an Electrodynamic Fine Spray. *Journal of Aerosol Science* 20 153-164
- Grace, J. and Marijnissen, J. (1994). A review of liquid atomization by electric means. *Journal of Aerosol Science* 25 (6) 1005-1019
- Grifoll-Taverna, J. and Rosell-Llompart, J. (2009). Modeling Electro spray Droplets Transport for Thin Film Formation. Catalans: Universitat Rovila
- Grimm, L. R. and Beauchamp, J. (2005). Dynamics of field induced droplet ionization: time-resolved studies of distortion, jetting, and progeny formation from charged and neutral methanol droplets exposed to strong electric fields. *Journal of Physical Chemistry B* 109 (16) 8244-8250
- Hartman, R. et al., (1998). The evolution of electrohydrodynamic sprays produced in the cone-jet mode, a physical model. *Journal of Electrostatics* 47 143-170
- Hartman, R. et al., (1999). Electrohydrodynamic atomization in the cone-jet mode: Physical modeling of the liquid cone and jet. *Journal of Aerosol Science* 30 (7) 823-849
- Hinds, W. C. (1999). *Aerosol Technology; Properties, behaviour, and measurement of airborne particles*. New York: John Wiley & Sons, Inc.
- Hoeve, W. et al., (2010). Breakup of diminutive Rayleigh jets. Massachusetts: American Institute of Physics (AIP)
- Klaseboer, E., Manica, R. and Chan, D. (2014). Universal behaviour of the initial stage of drop impact. *Physical Review Letters* 19 (194501) 113-117
- Lasheras, J. and Clanet, C. (1999). Transition from dripping to jetting. *Journal of fluid mechanics* 383 307-326
- Leornado, d. V. (1490). *The Codex Leicester*. Sydney: Powerhouse
- Lin, S. (2003). *Breakup of Liquid Sheets and Jets*. New York: Cambridge University Press
- Maxey, M. and Riley, J. (1993). Equation of motion for a small rigid sphere in a nonuniform flow. *Physics of Fluids* 26 883-889
- Plateau, J. A. F. (1873). *Statique expérimentale et théorique des liquides soumis aux seules forces moléculaires*. Paris: Gauthier-Villard

- Rayleigh, F. (1879). On the Capillary Phenomena of Jets. Proceedings of the Royal Society of London (1854-1905) 29 71-97
- Splung (2016). Illustrated Surface Charge Distribution in Electrostatics [online] available from: <<http://www.splung.com/content/sid/3/page/electrostatics>> [ 25 Jan 2016].
- Tang, K. and Gomez, A. (1994a). Charge and Fission of Droplets in Electrostatic Sprays, Physics of Fluids 6 (1) 404-414
- Tang, K. and Gomez, A. (1994b). On the structure of an electrostatic spray of monodisperse droplets. Physics of Fluids 6 (7) 2317-2332
- Taylor, G. (1969). Proceedings of the Royal Society of London. Mathematical and Physical Sciences 313 (1515) 453-475
- Tchen, C.M. (1947). Martinus Nijhoff. Phd Thesis, Delft University of Technology, Netherlands
- Wetzel, E. D. and Tucker, C. L. (1999). Droplet Deformation in Dispersions with Unequal Viscosities, Urbana-Champaign, Urbana: Dept. of Mechanical and Industrial Engineering University of Illinois
- Yurteri, C., Hartman, R. and Marijnissen, J. (2010). Production of Pharmaceuticals Particles via Electrospraying with an Emphasis on Nano and Nano Structured Particles-A Review. KONA Powder and Particle Journal (18) 91-115
- Zeleny, J. (1915). On the Conditions of Instability of electrified drops, with applications to electrical discharge at liquid points. London: Proceedings of Cambridge Philosophy Society
- Zhang, Z. and Chen, Q. (2007). Comparison of the Eulerian and Lagrangian methods for predicting particle transport in enclosed spaces. Atmospheric environment 25 5236-5248

## Appendix

The self-developed routines have been appended with their explanations. The main routines are Drop\_isolation and trace, while their subroutines are numbered in roman numbers.

1. Drop\_isolation
  - (i) Match\_drops
2. Trace
  - (i) Droplet\_seeding
  - (ii) Icforce
  - (iii) Evalallfdst
  - (iv) Dragfdst

### 1. Drop\_isolation

```
%Routine that isolates the individual droplets from the images
data=load('5 kV_460.txt'); %loading the text file from ImageJ, having the droplet position matrix
%initializing the parameters
rhog=1.2;eta=1.81e-5;
y=data(:,5); %existing y-coordinates
x=data(:,4); %existing x-coordinates
d=data(:,9); %corresponding Ferret sizes
slice=data(:,10); %associated slice
i=1;m=1;
while i<=length(y)-1 %matrix row size subtracted by one
    j=slice(i);
    ym(m,j)=y(i);
    xm(m,j)=x(i);
    dm(m,j)=d(i);
    i=i+1;
    m=m+1;
    if slice(i)>slice(i-1)
        m=1;
    end
end
matchdrops %Function that tracks droplets from one slide to the other
i=1; m=1;
while i<size(yn,1)
    j=1;
    n=1;
    while j<size(yn,2)
        Yn(m,n)=yn(i,j);
        Xn(m,n)=xn(i,j);
        Dn(m,n)=dn(i,j);
        if yn(i,j)==0
            while yn(i,j)==0
                j=j+1;
                if j>=size(yn,2)
                    break
                end
            end
            if n>1
```

```

        if yn(i,j+1)>0&&(yn(i,j+1)<Yn(m,n-1))
            n=0;
            m=m+1;
            break
        else if yn(i,j+1)>0&&(yn(i,j+1)>Yn(m,n-1))
            n=n-1;
            break
        end
    end
end
end
    j=j+1;
    n=n+1;
end
    i=i+1;
    m=m+1;
end
n=1;
Ynrws=size(Yn,1);
Ynclms=size(Yn,2);
for i=1:Ynrws
    if round(Yn(i,1))<=ceil(Yn(1,1))
        for j=1:size(Yn,2)
            Yn1(n,j)=Yn(i,j);
            Xn1(n,j)=Xn(i,j);
            Dn1(n,j)=Dn(i,j);
        end
        n=n+1;
    end
end
frate=12500;%input('Please enter the camera frame rate per second ');
tintv=1/frate;
i=1;time=zeros(1,size(Yn,2)-1);
vel=inline('((b-a)/t)','a','b','t');
while i<size(Yn1,1)
    j=1;
    while j<size(Yn1,2)-1
        A(i,j)=1e-3*(Xn1(i,j+1)-Xn1(i,j));
        B(i,j)=1e-3*(Yn1(i,j+1)-Yn1(i,j));
        S(i,j)=sqrt(A(i,j)^2+B(i,j)^2);
        velx(i,j)=1e-3*vel(Xn1(i,j),Xn1(i,j+1),tintv);
        vely(i,j)=1e-3*vel(Yn1(i,j),Yn1(i,j+1),tintv);
        velr(i,j)=S(i,j)*frate;
        if j>1
            if vely(i,j)>2||velr(i,j)>2||velx(i,j)>2
                velx(i,j)=velx(i,j-1);
                vely(i,j)=vely(i,j-1);
                velr(i,j)=velr(i,j-1);
            end
        else if i>1
            if vely(i,j)>2||velr(i,j)>2||velx(i,j)>2
                velx(i,j)=velx(i-1,j);
                vely(i,j)=vely(i-1,j);
                velr(i,j)=velr(i-1,j);
            end
        end
    end
end
end

```

```

        end
    if j>1
    time(1,j)=time(1,j-1)+tintv;
    end
    if Yn1(i,j)==0||Yn1(i,j+1)==0
        vely(i,j)=0;
    end
    if Xn1(i,j)==0||Xn1(i,j+1)==0
        velx(i,j)=0;
    end
    j=j+1;
    end
    i=i+1;
    end
    g=0;
    for iv=1:size(vely,1)-1
    if vely(iv,1)>0
        g=g+1;
        for j=1:size(vely,2)-1
            Velcx(g,j)=velx(iv,j);
            Velcy(g,j)=vely(iv,j);
            Velcr(g,j)=velr(iv,j);
        end
    else if vely(iv,2)>0
        g=g+1;
        for j=2:size(vely,2)-1
            Velcx(g,j-1)=velx(iv,j);
            Velcy(g,j-1)=vely(iv,j);
            Velcr(g,j-1)=velr(iv,j);
        end
    end
    end
    end
    int=1;
    for n=1:size(Velcy,2)
        j=1;
        for i=1:size(Velcy,1)
            velX(j,n)=Velcx(i,n);
            velY(j,n)=Velcy(i,n);
            velR(j,n)=Velcr(i,n);
            ReynoldX(j,n)=1e-3*abs(velX(j,n))*Dn1(j,n)*rhog/eta;
            ReynoldY(j,n)=1e-3*abs(velY(j,n))*Dn1(j,n)*rhog/eta;
            ReynoldR(j,n)=1e-3*abs(velR(j,n))*Dn1(j,n)*rhog/eta;
            j=j+1;
            if i==size(Velcy,1)
                velX(j:i,n)=Velcx(i,n);
                velY(j:i,n)=Velcy(i,n);
                velR(j:i,n)=Velcr(i,n);
            end
        end
    end
    end
    hold off
    XN=Xn';
    XN(~XN)=nan;
    YN=Yn';
    YN(~YN)=nan;
    DN=Dn';

```

```

DN(~DN)=nan;
hold on
fig1=figure;
for i=1:size(XN,2)
    plot(-XN(1:size(XN,1),i),-YN(1:size(YN,1),i))
    hold on
end
title('-6 kV at 285mL h-1 2 m s-1 from breakup','FontSize',14)
xlabel('Horizontal axis (mm)','FontSize',12)
ylabel('Vertical axis (mm)','FontSize',12)
plot(YN(1:size(XN,1),1:100),DN(1:size(YN,1),1:100))
save('c:\mymfiles\Matlab_expedata\9kV_285mL_h','YN','XN','DN')

```

### (i) Match\_drops

```

%Routine that matches the droplets from one slide to the next
%Initialization of parameters
j=1; L=1; count=0; bk2=0;chk=0;
yn=zeros(size(ym));xn=zeros(size(xm));dn=zeros(size(dm));
while bk2==0&&j<size(ym,2)
    i=1; bk1=0;
    while bk1==0 && i<=size(ym,1)
        i1=1; bk=0;flg=0;chk1=zeros;
        if j==1
            yn(i,j)=ym(i,j);
            xn(i,j)=xm(i,j);
            dn(i,j)=dm(i,j);
        else if j>1
            while bk==0;
                YX(:,1)=ym(:,j);
                YX(:,2)=xm(:,j);
                YX(:,3)=dm(:,j);
                xy=YX;%sortrows(YX,1);
                xy(~xy)=nan;
                if j==2||i==1
                    if yn(i,j-1)<xy(i1,1)&&(round(xn(i,j-1))==round(xy(i1,2)))&&(abs(xn(i,j-1)-
                    xy(i1,2))<abs(yn(i,j-1)-xy(i1,1)))
                        yn(i,j)=xy(i1,1);
                        xn(i,j)=xy(i1,2);
                        dn(i,j)=xy(i1,3);
                        bk =1;
                    end
                    else if (j>2)&&(yn(i,j-1)<xy(i1,1))&&(yn(i,j-1)~=0)&&(abs(((xn(i,j-1)-xn(i,j-2))-
                    ((xy(i1,2)-xn(i,j-1))))<0.5)&&(abs(((yn(i,j-1)-yn(i,j-2))-((xy(i1,1)-yn(i,j-1))))<0.5)
                        yn(i,j)=xy(i1,1);
                        xn(i,j)=xy(i1,2);
                        dn(i,j)=xy(i1,3);
                        bk =1;
                    else if (j>2)&&(yn(i,j-1)<xy(i1,1))&&(yn(i,j-1)==0)
                        yn(i,j)=xy(i1,1);
                        xn(i,j)=xy(i1,2);
                        dn(i,j)=xy(i1,3);
                        if yn(i,j-1)==0 &&yn(i,j)~=0
                            flg=flg+1;
                            chk1(flg)=i;
                        end
                        bk =1;
                    end
                end
            end
        end
    end
end

```

```

else if (j>2)&&(yn(i,j-2)==0)&&(yn(i,j-1)<xy(i1,1))%&&(round(xn(i,j-
1))==round(xy(i1,2)))
    yn(i,j)=xy(i1,1);
    xn(i,j)=xy(i1,2);
    dn(i,j)=xy(i1,3);
    bk =1;
end
end
end
end
    i1=i1+1;
    if i1>length(xy)
        bk=1;
    end
end
end
end
    i=i+1;
    if flg>=1
        for r=1:flg
            tst=1;
            chk=chk1(r);
            while tst<chk
                if (yn(chk,j)==yn(tst,j))&&(tst~=chk)
                    yn(chk,j)=0;
                    xn(chk,j)=0;
                    dn(chk,j)=0;
                    chg(j)=chk;
                end
                tst=tst+1;
            end
            tst=tst+1;
            while (tst<size(ym,1))
                if (yn(chk,j)==yn(tst,j))&&(tst~=chk)
                    yn(chk,j)=0;
                    xn(chk,j)=0;
                    dn(chk,j)=0;
                    chg(j)=chk;
                end
                tst=tst+1;
            end
        end
    end
end
end
end
    j=j+1;
end

```

## 2. Trace

```

%Routine that solves the force balance equation for all droplets
es=load ('pot_-5 kV_plate_A.txt');%loading the background electric field matrix
%initializing the parameters
flowrate=285;
L_breakup=8.0e-3;
T=8/12500;
vj=1.1;
Re_limit=0.01*2.5; %Rayleigh limit
davg= 600e-6;

```

```

[m,n] = size(es); ES=es; es=sortrows(ES,[1 2]);
x=es(1:m,1); y=es(1:m,2); ex= es(1:m,3);ey= es(1:m,4);
rho=1e3; gvt=9.81; rhog=1.2; eta=1.81e-5; mew=1e-3; gamma=7.19e-2;
epsilon0=8.8542e-12; er=8.01e1; epsilon=epsilon0*er; time=0; checkvalue=0; timer1=0;np=1;
frate=flowrate*(1e-6)/(3600);% the flowrate is in mL h-1
Dvolavg=(pi*davg^3)/6;
tintv=(0.2/(frate/(Dvolavg))); %defining time interval
np1=round(1/tintv);
tim=zeros(1,200);
    Droplet_seeding_285 %function for droplet seeding
    Xp=80*1e-3; Yp=(62.5-0.5*L_breakup*1000+tintv*vj*5*1000)*1e-3;
    Xin=80;
    Yin=62.5-L_breakup*1000; %position of the breakup point on the defined geometry
    Ux=0;
    Uy=-vj;
    np_count=1; t=1;
while ((max(Xin(t,1:np))>-120)&&(max(Yin(t,1:np))>-
220))&&((max(Xin(t,1:np))<280)&&(max(Yin(t,1:np))<95))&&((Xin(t,np)~=0)&&(Yin(t,np)~=0))&
&(np_count<100)% loop for seeding 100 droplets
    if (timer1==5)&&(np_count<np1)%calculating droplet displacement 5 times
        timer1=0;
        np_count=np_count+1;
        np=np_count;
        Droplet_seeding_285 %function for droplet seeding
        Xin(t,np_count)=80;
        Yin(t,np_count)=62.5-L_breakup*1000;
        Ux(t,np_count)=0;
        Uy(t,np_count)=-vj;
    end
    timer1=timer1+1;
    icforce
for np=1:np_count
    X=zeros(t,np);
    Y=zeros(t,np);
    X(t,np)=1e3*X1(t,np);
    Y(t,np)=1e3*Y1(t,np);
        if (X(t,np)<-120)||(Y(t,np)<-220)||(X(t,np)>280)||(Y(t,np)>95)
            Yin(t+1,np)=Yin(t,np);
            Xin(t+1,np)=Xin(t,np);
            Uy(t+1,np)=0;
            Ux(t+1,np)=0;
            q(np)=0;
        else if (X(t,np)>-120)&&(Y(t,np)>-
220)&&(X(t,np)<280)&&(Y(t,np)<95)&&(X(t,np)~=0)&&(Y(t,np)~=0)
            i=0;j=0;p=0;
for g=1:m
            if ((round(x(g))==round(X(t,np))))&&((round(y(g))==round(Y(t,np))))
                h=g;
                p=p+1;
            end
            if (g>1)&&(round(x(g-1))==round(X(t,np))&&(round(x(g))~=round(X(t,np)))
                for k=h:h+p
                    if (roundn(x(k),-2)==roundn(X(t,np),-2))&&(roundn(y(k),-2)==roundn(Y(t,np),-2))
                        Evalallfdst
                        break
                    end
                end
            end
end
end

```



```

if j~=0
    break
end
for k=h:h+p
    if (roundn(x(k),-2)==roundn(X(t,np),-2))&&(roundn(y(k),-1)==roundn(Y(t,np),-1))
        Evalallfdst
        break
    end
end
if j~=0
    break
end
for k=h:h+p
    if (roundn(x(k),-1)==roundn(X(t,np),-1))&&(roundn(y(k),-2)==roundn(Y(t,np),-2))
        Evalallfdst
        break
    end
end
if j~=0
    break
end
for k=h:h+p
    if (roundn(x(k),-1)==roundn(X(t,np),-1))&&(roundn(y(k),-1)==roundn(Y(t,np),-1))
        Evalallfdst
        break
    end
end
if j~=0
    break
end
for k=h:h+p
    if (roundn(x(k),-1)==roundn(X(t,np),-1))&&(round(y(k))==round(Y(t,np)))
        Evalallfdst
        break
    end
end
if j~=0
    break
end
for k=h:h+p
    if (round(x(k))==round(X(t,np)))&&(roundn(y(k),-1)==roundn(Y(t,np),-1))
        Evalallfdst
        break
    end
end
if j~=0
    break
end
for k=h:h+p
    if (round(x(k))==round(X(t,np)))&&(round(y(k))==round(Y(t,np)))
        Evalallfdst
        break
    end
end
if j~=0
    break
end
end

```

```

        end
    end
end
    end
end
    end
t=t+1
end
t1=1;
for i=1:np
    plot(Xin(t1:t-2,i),Yin(t1:t-2,i),'-b')
    t1=t1+5;
    hold on
end

```

### (i) Droplet\_seeding

%Routine seeds the droplets one after the other with a defined size distribution

```

if rem(np,10)==1
    d(np)=500e-6+40e-6*rand(1);
    else if rem(np,10)==7
        d(np)=540e-6+40e-6*rand(1);
    else if rem(np,10)==2 ||rem(np,10)==5||rem(np,10)==4
        d(np)=580e-6+50e-6*rand(1);
    else if rem(np,10)==3 ||rem(np,10)==6 ||rem(np,10)==9
        d(np)=630e-6+70e-6*rand(1);
    else if rem(np,10)==8
        d(np)=700e-6+50e-6*rand(1);
    else if rem(np,10)==0
        d(np)=730e-6+150e-6*rand(1);
    end
    end
    end
    end
end
    qR(np)=sqrt(8*pi^2*epsilon0*gamma*d(np)^3);
    q(np)=Re_limit*qR(np);
    Dvol(np)=(pi*d(np)^3)/6; mass(np)=Dvol(np)*rho;

```

### (ii) Icforce

%Routine that calculates the coulombic force of interaction between droplets for and due to all droplets

```

X1(t,1:np)=1e-3*(Xin(t,1:np));
Y1(t,1:np)=1e-3*(Yin(t,1:np));
Fctx(t,1:np)=0;
Fcty(t,1:np)=0;
Fcou=inline('q1*q2/(4*pi*8.8542e-12*r^2)','q1','q2','r');
    Fcx=zeros(np,np);
    Fcy=zeros(np,np);
for i1=1:np
for j1=1:np
    if j1~=i1 && ((q(i1)~=0)|| (q(j1)~=0))
        if j1<i1
            cx(i1,j1)=X1(j1)-X1(i1);
            cy(i1,j1)=Y1(j1)-Y1(i1);
            r(i1,j1)=sqrt((cx(i1,j1))^2+(cy(i1,j1))^2);

```

```

teta(i1,j1)=atand((cy(i1,j1))/(cx(i1,j1)));
Cx=cx(i1,j1);
Cy=cy(i1,j1);
if (Cx<0)&&(Cy<0)
    teta(i1,j1)=teta(i1,j1)-180;
else if (Cx<0)&&(Cy>0)
    teta(i1,j1)=teta(i1,j1)+180;
else if (Cx<0)&&(Cy==0)
    teta(i1,j1)=teta(i1,j1)-180;
end
end
end
Fcx(i1,j1)=Fcoul(q(i1),q(j1),r(i1,j1))*cosd(teta(i1,j1));
Fcy(i1,j1)=Fcoul(q(i1),q(j1),r(i1,j1))*sind(teta(i1,j1));
Fctx(t,i1)=(Fctx(t,i1)+Fcx(i1,j1));
Fcty(t,i1)=(Fcty(t,i1)+Fcy(i1,j1));
else if j1>i1
cx(i1,j1-1)=X1(j1)-X1(i1);
cy(i1,j1-1)=Y1(j1)-Y1(i1);
r(i1,j1-1)=sqrt((cx(i1,j1-1))^2+(cy(i1,j1-1))^2);
teta(i1,j1-1)=atand((cy(i1,j1-1))/(cx(i1,j1-1)));
Cx=cx(i1,j1-1);
Cy=cy(i1,j1-1);
if (Cx<0)&&(Cy<0)
    teta(i1,j1-1)= teta(i1,j1-1)-180;
else if (Cx<0)&&(Cy>0)
    teta(i1,j1-1)=teta(i1,j1-1)+180;
else if (Cx<0)&&(Cy==0)
    teta(i1,j1-1)=teta(i1,j1-1)-180;
end
end
end
Fcx(i1,j1-1)=Fcoul(q(i1),q(j1),r(i1,j1-1))*(cosd(teta(i1,j1-1)));
Fcy(i1,j1-1)=Fcoul(q(i1),q(j1),r(i1,j1-1))*(sind(teta(i1,j1-1)));
Fctx(t,i1)=(Fctx(t,i1)+Fcx(i1,j1-1));
Fcty(t,i1)=(Fcty(t,i1)+Fcy(i1,j1-1));
end
end
end
cx_jet(i1)=Xp-X1(i1);
cy_jet(i1)=Yp-Y1(i1);
r_jet(i1)=sqrt(cx_jet(i1)^2+cy_jet(i1)^2);
teta_jet(i1)=atand(cy_jet(i1)/cx_jet(i1));
Cx_jet=cx_jet(i1);
Cy_jet=cy_jet(i1);
if (Cx_jet<0)&&(Cy_jet<0)
    teta_jet(i1)=teta_jet(i1)-180;
else if (Cx_jet<0)&&(Cy_jet>0)
    teta_jet(i1)=teta_jet(i1)+180;
else if (Cx_jet<0)&&(Cy_jet==0)
    teta_jet(i1)=teta_jet(i1)-180;
end
end
end
Q_jet=10*q(i1);
Fcx_jet(i1)=Fcoul(q(i1),Q_jet,r_jet(i1))*(cosd(teta_jet(i1)));

```

```

Fcy_jet(i1)=Fcoul(q(i1),Q_jet,r_jet(i1))*(sind(teta_jet(i1)));
Fctx(t,i1)=(Fctx(t,i1)+Fcx_jet(i1));
Fcty(t,i1)=(Fcty(t,i1)+Fcy_jet(i1));

```

end

### (iii) Evalallfdst

% Finds the resultant force and solves the kinematic equations for each droplet

% obtains the new position and new velocity

```

velf=inline('u+a*t','u','a','t');
dis=inline('u*t+0.5*a*t^2','u','a','t');
Fe=inline('e*q','e','q');
Fex(t,np)=Fe(ex(k),q(np));
Fey(t,np)=Fe(ey(k),q(np));
Fg(np)=-mass(np)*gvt;
Dragfdst %function calculating drag force
Fxt(np)=Fex(t,np)+Fctx(t,np)+FDx(t,np);
Fyt(np)=Fey(t,np)+Fcty(t,np)+Fg(np)+FDy(t,np);
ax1(t,np)=Fxt(np)/mass(np);
ay1(t,np)=Fyt(np)/mass(np);
j=j+1;
time(t+1)=time(t)+tintv;
if rem(np,2)==0
tim(1,np)=tim(np)+tintv;
else
tim(1,np)=tim(np)-tintv;
end
Ux(t+1,np)=velf(Ux(t,np),ax1(t,np),tintv);
Uy(t+1,np)=velf(Uy(t,np),ay1(t,np),tintv);
Xin(t+1,np)=Xin(t,np)+1e3*dis(Ux(t,np),ax1(t,np),tintv);
Yin(t+1,np)=Yin(t,np)+1e3*dis(Uy(t,np),ay1(t,np),tintv);

```

%The model takes constant time steps

### (iv) Dragfdst

% The routine receives the droplet's size and velocity, obtains the Reynold's number, and the Drag force

```

FDx(t,np)=0;
FDy(t,np)=0;
FDrgS=inline('3*pi*1.81e-5*d*(0-v)','d','v');
FDrgN=inline('(pi/8)*CD*1.20*d^2*abs(v)*(0-v)','CD','d','v');
Reynold=inline('66000*d*v','d','v');
cd=inline('(24/Re)*(1+0.15*(Re^0.687))','Re');
velmag=inline('sqrt(vx^2+vy^2)','vx','vy');
U=velmag(Ux(t,np),Uy(t,np));
Re(t,np)=Reynold(d(np),U);
if (Re(t,np)>1)&&(Re(t,np)<1000)
CD(t,np)=cd(Re(t,np)); % obtaining drag coefficient
FDx(t,np)=FDrgN(CD(t,np),d(np),Ux(t,np));%finding drag force x-component
FDy(t,np)=FDrgN(CD(t,np),d(np),Uy(t,np));%finding drag force y-component
else
FDx(t,np)=FDrgS(d(np),Ux(t,np));
FDy(t,np)=FDrgS(d(np),Uy(t,np));
end

```

% The model assumes perfect spheres